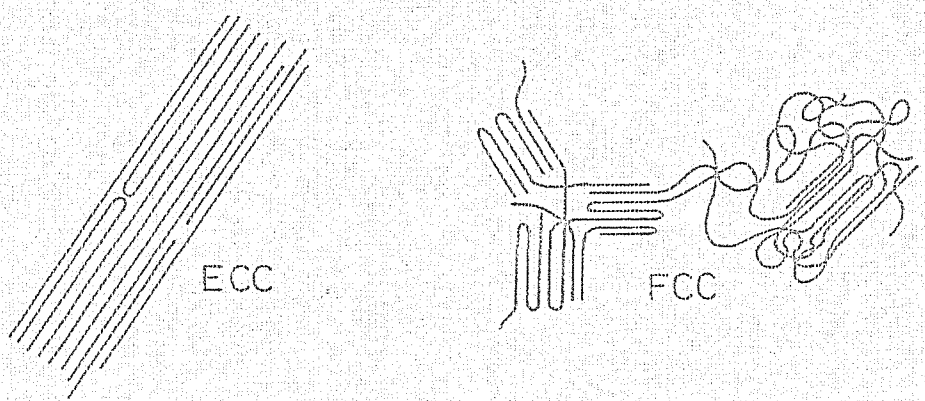
A Study on Orientation-Induced Crystallization in Two-Phase Polymer Melt Systems

C.L.J.A. Verbraak



TR diss
1686

ברזילי
דוקטורט
TA diss 1694

A Study on Orientation-Induced Crystallization in Two-Phase Polymer Melt Systems

A Study on Orientation-Induced Crystallization in Two-Phase Polymer Melt Systems

Proefschrift

BIBLIOTHEEK TECHNISCHE UNIVERSITEIT
Prometheusplein 1
DELFT

ter verkrijging van de graad van doctor
aan de Technische Universiteit Delft
op gezag van de Rector Magnificus,
Prof.drs. P.A. Schenk
in het openbaar te verdedigen
ten overstaan van een commissie aangewezen
door het College van Dekanen
op dinsdag 29 november 1988 te 14.00 uur door

Constantinus Leonardus Jozef Andre Verbraak
scheikundig ingenieur
geboren te Rotterdam

TR diss
1686

Dit proefschrift is goedgekeurd door de promotor

Prof.dr.ir. A.K. van der Vegt

Voor Anita
en m'n ouders

Met dank aan allen die hun bijdrage hebben geleverd aan het tot stand komen van dit proefschrift; allereerst de Stichting voor de Technische Wetenschappen voor financiële ondersteuning, en verder met name: Jaap van Dam, Fred van Dijk, Arjen Dijkgraaf, Piet Dullaart, Fred Hammers, Richard van Hoeven, Ton Keijzers, Harry van Loon, Henk Nieuwpoort, Klaas te Nijenhuis, Jaap Raadsen, Ruud Tijssens, Anne van der Vegt en Gerard de Vos.

Contents

	page
1 Introduction	**1**
2 Methods to obtain orientation in flexible-chain polymers	**3**
2.1 *Solid state extrusion*	3
2.2 *Hydrostatic extrusion*	4
2.3 *Hot drawing*	5
2.4 *Polymerization of monomer single crystals*	6
2.5 *Simultanuous crystallization and polymerization of monomers*	6
2.6 *Zone-annealing*	7
2.7 *Orientation-induced crystallization of entangled networks from solution*	8
2.8 *Gel spinning*	10
3 Description and analysis of the process: orientation-induced crystallization in two-phase polymer flow	**11**
3.1 *Introduction*	11
3.2 *Process options*	14
3.3 *Analysis of the process*	15
3.3.1 *The time scale of the experiment*	16
3.3.2 *The relaxation time scale*	16
3.3.3 *The crystallization time scale*	17
4 Deformational behaviour of two-phase molten polymer systems	**19**
4.1 *Introduction*	19
4.2 *Cocontinuous two-phase systems*	19
4.2.1 *Newtonian fluids*	20
4.2.2 *Second order fluids*	23
4.2.3 *Power law fluids*	25

4.3 *Experimental observations of the coextrusion diameter ratio* 27
4.3.1 *Equipment* 27
4.3.2 *Materials* 29
4.3.3 *Results* 30
4.3.4 *Discussion* 31
4.4 *Dispersed two-phase systems* 34
4.4.1 *Introduction* 34
4.4.2 *Fiber formation* 35
4.4.3 *Rheological parameters* 37
4.5 *Experimental investigation of fiber formation conditions* 41
4.5.1 *Equipment and method* 41
4.5.2 *Materials* 42
4.5.3 *Results* 42

5 The relaxation behaviour of a stretched polymer melt **46**

5.1 *Introduction* 46
5.2 *Theoretical models* 46
5.2.1 *Lodge's constitutive equation* 47
5.2.2 *Wagner's constitutive equation* 49
5.3 *Experiments* 51
5.4 *Results* 53
5.4.1 *Stress build-up and relaxation* 53
5.4.2 *The relaxation time spectrum* 55
5.4.3 *Comparison with Lodge's constitutive equation* 57
5.4.4 *Discussion* 57
5.4.5 *Comparison with Wagner's constitutive equation* 59
5.4.6 *Discussion* 60

6 Scouting experiments **63**

6.1 *Batch-wise coextrusion* 63
6.2 *Continuous coextrusion* 65
6.3 *Batch-wise extrusion of dispersions* 71
6.4 *Milling of dispersions* 74

7 Conclusions **77**

References **80**

Summary **84**

Samenvatting **85**

List of symbols **86**

1 Introduction

An important disadvantage of polymer materials is their relative weakness: the covalent carbon-carbon-bond is the strongest of all (think, for instance, of the remarkably good mechanical properties of diamond), but although most technical polymer chains are built out of such a carbon-carbon backbone, the macroscopic material reaches only a fraction of its theoretical strength and stiffness.

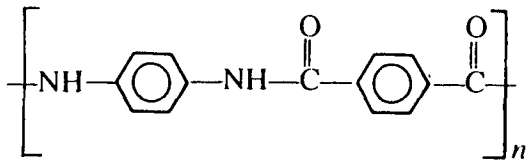
The main reason for this behaviour is the fact that under normal conditions polymer chains, being built up out of flexible units, will not be present in a stretched configuration. Due to entropic factors these very long molecules will coil and bend together to form a highly entangled ball, both in solution and melt. On solidification, in the case of amorphous polymers this configuration will be frozen in in the solid state. In the case of semi-crystalline polymers this configuration has to change in such a way that the molecules fit into the crystal lattice. Also in this case the molecules will not be incorporated within the crystal in a stretched configuration.

As a result of these factors, under load these materials cannot exhibit mechanical properties that even get near the values for the covalent carbon-carbon bond; for instance, the theoretical value for the stiffness of polyethylene (a carbon-carbon backbone in the well-known zig-zag configuration without side-chains) in the direction of chain orientation reaches 255 GPa ($= 255 \cdot 10^9$ N/m^2), but the stiffness of conventional polyethylene is only in the order of 1 or 2 GPa.

Several possibilities exist to cope with this technological challenge. Two routes can mainly be chosen: one can take a polymeric material in which the backbones are not flexible like in polyethylene, or one can try to process the flexible-chain polymer in such a way that the chains are mainly oriented in the desired direction. In these cases, factors like chain length and Van der Waals' interactions between chains influence the ultimate mechanical properties (mainly the tensile strength) to a large extent.

Examples of a successful result of the first route are the Kevlar and Twaron fiber materials, made out of aromatic polyamides. The chemical

structure of these compounds is as follows:



The aromatic groups incorporated in the polymer backbone are responsible for the rigidness of the molecule. Therefore these molecules will, in solution, behave like rods and exhibit a liquid-crystalline behaviour. Even very mild flow conditions will yield an alignment of the rigid molecules in the flow direction, and approximate values for the mechanical properties of the resulting fiber are a tensile strength of 3 GPa and a Young's modulus of 65 GPa. Recently a new class of liquid crystalline polymers has been introduced on a commercial scale; these materials do not have to be spun from solution, but can be processed directly from the melt. They are called "thermotropic polymers". This allows for the manufacturing of larger, homogeneous (but not isotropic!) parts, for instance by extrusion or injection moulding, that exhibit very good mechanical properties. Unfortunately, processing of these materials caused a number of problems that can not be dealt with by the common knowledge in polymer technology. Furthermore, the high price is a reason for the fact that only very specialized applications of thermotropic polymers have been found until now.

The second route to produce strong and stiff polymer structures, viz. that of high orientation of flexible chain molecules, has been a subject of research throughout the last two decades. Fiber spinning is perhaps the oldest technological solution to this problem, and the quality of as-spun synthetic fibers is still improving. Nevertheless, many scientists were not satisfied with the properties that can be reached by simple fiber spinning, and numerous methods to increase the degree of molecular orientation in the resulting product have been investigated. A few examples of more or less successful methods will be given in the next chapter.

2 Methods to obtain orientation in flexible-chain polymers

Without claiming to be complete, in this chapter a review of methods to obtain a high degree of orientation in polymers that are built out of flexible-chain molecules is presented in arbitrary order.

2.1 *Solid state extrusion*

The principle of this process is the plastic deformation of flexible-chain polymers just under their melting point [1-3]. Using extremely high pressures, a solid thermoplastic mass is forced through a conical die. Under these circumstances very high shear stresses are generated, due to which the polymer material softens to a certain extent (shear-induced melting). This allows for the realisation of a continuous process with a production speed of approximately 0.5 cm/min.

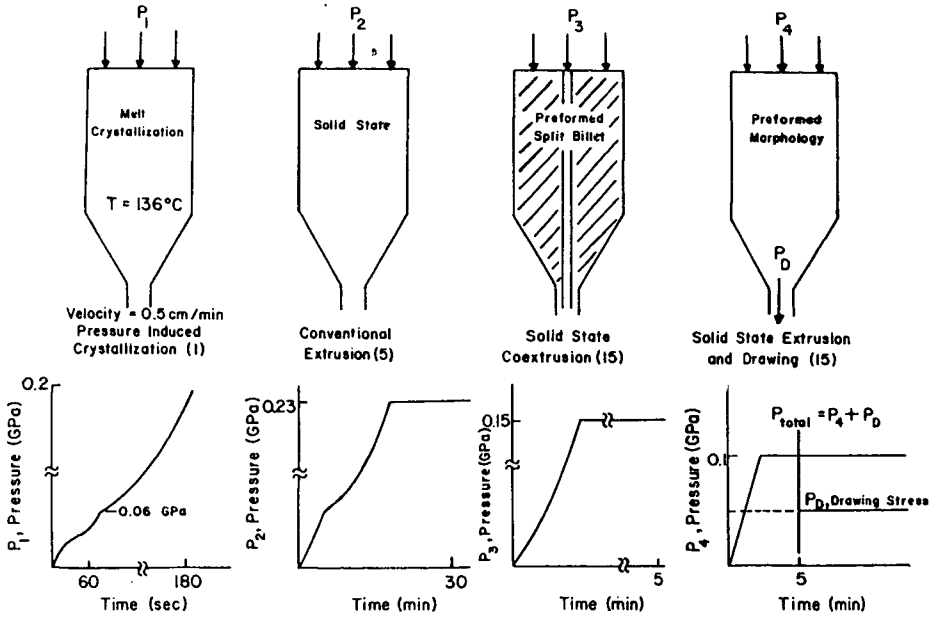


Fig.2.1 Schematic representation of processing conditions in solid state extrusion.

The process conditions (mainly the temperature, [4]) are very critical; the pressure sometimes rises dramatically, making extrusion with a constant speed impossible [5]. This problem can be partially overcome by improving the crystal morphology of the starting material [6]; by controlled crystallisation imperfections like air inclusions and shrinkage voids can be avoided while creating a very regular spherulitic structure.
Also, processing at lower pressures can be realized by using preformed split billets as a starting material, thereby creating free surfaces in the longitudinal direction.
The resulting mechanical properties of the products made by the solid-state extrusion process are [1,7-10] for polyethylene a Young's modulus of 70 GPa and a tensile strength of 0.6 GPa (theoretical maximum 30 GPa). A schematic representation of the main process characteristics is given in figure 2.1.

2.2 *Hydrostatic extrusion*

In this process, which is also used for forming metals, a solid plug of a semi-crystalline thermoplastic polymer is forced through a converging channel just under its melting point and surrounded by a lubricating fluid. Also, this fluid is responsible for transferring the necessary extrusion pressure, as can be seen in figure 2.2.

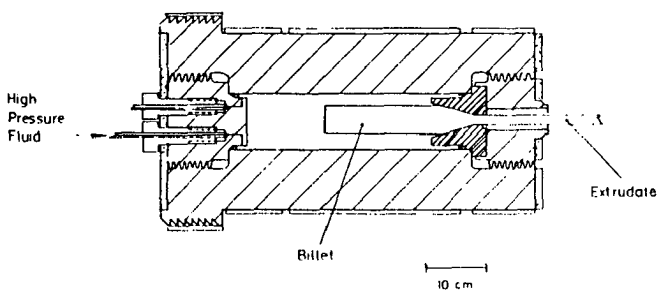


Fig.2.2 Schematic drawing of the hydrostatic extrusion equipment.

Like in conventional extrusion the materials, used in this process, exhibit die-swell. Consequently the actual extrusion ratio, defined as

the ratio of the original billet and final product cross-sections, is the main process parameter.
The main advantage of this method over direct solid state extrusion is the elimination of the friction between the polymer plug and container walls and a decrease in the friction between the billet and the die, due to an entrained film of fluid. Furthermore, like in solid state extrusion, the possible end deformations are mainly determined by the geometry of the equipment used and not by material properties and/or process dynamics. Also products of larger diameters can be manufactured.
Experiments performed by Ward and coworkers [11,12] with linear polyethylene, using pressures up to 250 MPa, gave products with a Young's modulus of 60 GPa.

2.3 *Hot drawing*

While studying the influence of molecular weight and its distribution on the drawing behaviour of linear polyethylene (LPE), Ward and coworkers found that the so-called "natural draw ratio" (which is the highest possible degree of plastic deformation at room temperature) depends on the weight-average molecular weight: samples of relatively low molecular weight ($\bar{M}_w$ = 40,000-53,000) can be deformed to higher draw ratios (l/l_0 = 11-13) than samples of higher molecular weight ($\bar{M}_w$ = 80,000-200,000; l/l_0 = 7-10). For the latter range the natural draw ratio is more or less constant.
The mechanical properties of the drawn filaments show a very high correlation between the draw ratio and Young's modulus; the stiffness increases linearly from about 4 GPa at a draw ratio of 7 to about 20 GPa at a draw ratio of 13. If this tendency is to be extrapolated, it would be interesting to modify the process in such a way that higher draw ratios can be reached. Indeed it became clear [13,14] that it is possible to avoid formation of micro-cracks at temperatures above room temperature, but still under the melting point of the polymer, and thus to reach higher draw ratios ($l/l_0 \approx 20$).

The resulting, highly oriented LPE fibers [15] exhibit a Young's modulus of about 40 GPa. Furthermore, by giving the starting material several kinds of heat treatments with LPE draw ratios of 30 can be reached, the resulting fiber having a Young's modulus of 70 GPa which is in the same order of magnitude as that of aluminium or glass.
Following the same route with polypropylene (PP) draw ratios of 18 and higher and Young's moduli of 18 GPa (normally 1.4 GPa; theoretical maximum 42 GPa) can be reached. For polyoxymethylene (POM) the results are draw ratios of 25 and Young's moduli of 40 GPa (normally 2.8 GPa). Earlier, Clark and Scott [16] produced POM fibers with Young's moduli of 35 GPa by means of a drawing process in two stages.

2.4 *Polymerization of monomer single crystals*

In this technique macroscopic fully crystalline, chain-extended polymer single crystals are prepared by crystallizing the monomers in suitable morphological forms and then polymerizing the monomer crystals using heat, UV light or ionizing radiation [17,18]. Fibers up to 40 mm long with diameters of 10-100 μm can be prepared. Typical monomers for this technique are: 2,4-hexadiyne-1,6-diol *bis* (ethyl urethane), 2,4-hexadiyne-1,6- *bis* carbazol and 2,4-hexadiyne-1,6-diol *bis* (p-toluene sulphate). The resulting fibers have a Young's modulus of about 40 GPa, and no stress relaxation is observed.

2.5 *Simultanuous crystallization and polymerization of monomers*

Although closely related to the technique described in section 2.4 the different nature of the polymer under concern justifies a separate discussion of Iguchi's work [19]: needle crystals of polyoxymethylene (POM), 5-20 μm long, are formed during polymerization of trioxane in cyclohexane. Nucleation agents like $BF_3 \cdot OEt_2$ enhance extended-chain crystallization with the orientation parallel to the longitudinal direction of the needles. Characterization is only given by means of the melting temperature: 191.5°C compared to the normal value for POM of 181°C.

2.6 *Zone-annealing*

In this technique, developed in Japan by Kunugi and coworkers [20], the polymer samples are subjected to a two-stage treatment: first zone-drawing, followed by zone-annealing. In this process polymers like polyethylene terephthalate (PETP), nylon-6, polypropylene (PP) and polyethylene (PE) can be used. The two stages proceed as follows: During zone-drawing a band heater is moved with a constant speed (for instance 40 mm/min) along a polymer fiber which is clamped on both sides. The fiber can easily be stretched to 2.5-3.5 times its original length; characteristic temperatures are 90°C for PETP and 80°C for nylon-6.

The process of zone-annealing is performed with aid of the same equipment; parameters like temperature, band heater speed, fiber tension and the number of subsequent treatments are considered of main importance.

As a result of preliminary experiments the following conditions are proposed for PETP and nylon-6:

		PETP	Nylon-6
Temperature	(°C)	200-210	175
Heater speed	(mm/min)	10	10
Fiber tension	(GPa)	0.15-0.16	0.09-0.10
Number of treatments	(-)	5	5

Resulting mechanical properties are:

For PETP a Young's modulus of 18.0 GPa (normally 5.8 GPa, theoretical maximum 108 GPa) and a tensile strength of 0.9 GPa (normally 0.3 GPa); For Nylon-6 a Young's modulus of 8.3 GPa (normally 3.7 GPa, theoretical maximum 165 GPa) and a tensile strength of 1.0 GPa (normally 0.5 GPa).

Using almost the same technique, Yamada and coworkers [21] obtain a Young's modulus for polypropylene of 15 GPa (theoretical maximum 42 GPa).

2.7 *Orientation-induced crystallization of entangled networks from solution*

In this technique highly oriented fibers are produced from very dilute solutions by subjecting them to different flow fields. The orientation and subsequent crystallization are hydrodynamically induced; the long polymer chains are stretched while being incorporated in the crystal lattice. Very long molecules can be stretched effectively, especially when they are entangled in a network.
Using an adapted Czochralski's method, which consists essentially of pulling a crystal seed from a melt with a speed that is equal to the crystal growth rate, two methods were developed: Fiber growth in Poiseuille flow (figure 2.3) and in Couette flow (figure 2.4).

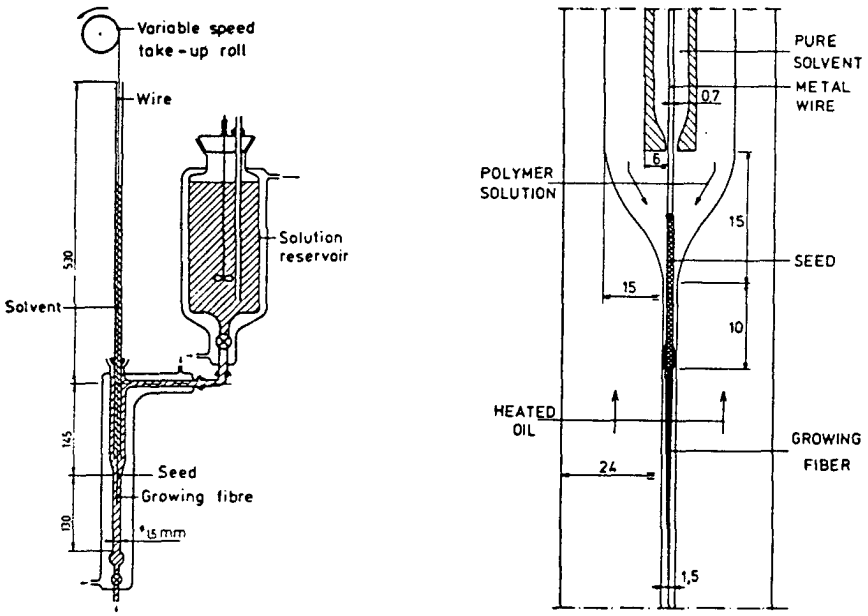


Fig.2.3 Continuous fiber growth in Poiseuille flow.

If polyethylene crystal seeds of 2 cm length were mounted in the entrance of a capillary, through which a supercooled solution of ultra-high molecular weight polyethylene (UHMWPE) in p-xylene was allowed to flow, after an incubation period crystal growth in the longitudinal direction could be observed. When this growing fiber is pulled up with a speed, adapted to the crystal growth rate, continuous production of a macro-fiber can be realized [22-25].

A discussion of fiber growth in Couette flow (figure 2.4) should distinguish between two possible mechanisms, namely free growth and surface growth.

In the case of free growth the crystal seed is situated exactly in the middle of the spacing between inner and outer cylinder of the Couette apparatus. This situation can be directly compared with the mechanism in Poiseuille flow, as described above. In the case of surface growth the crystal seed is situated at the surface of the rotor, which essentially is the inner cylinder of the Couette apparatus. Growth

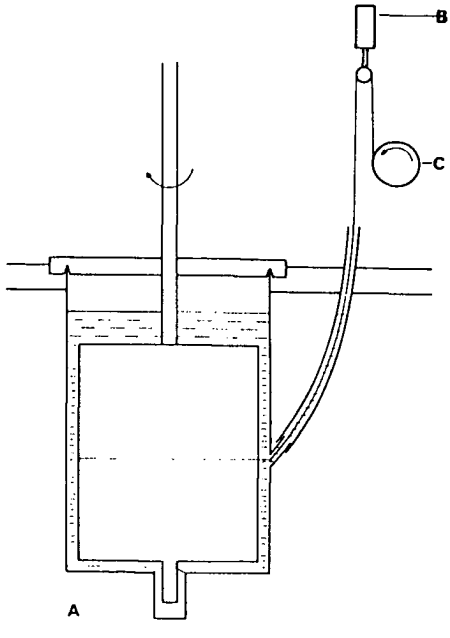


Fig.2.4 Continuous fiber growth in Couette flow.

rates of 150 cm/min at 123 °C can be realized with this method [26].
The fibers produced with these methods exhibit the following mechanical properties: Young's moduli up to 100 GPa and tensile strengths up to 4 GPa. These results can even be improved by hot-drawing the fibers as produced in the Couette-apparatus [27,28]: Young's moduli up to 106 GPa and tensile strengths up to 4.7 GPa can be reached.
Especially the high tensile strength of these polyethylene fibers (compared to the fibers made by solid state extrusion, hydrostatic extrusion and/or hot-drawing) is remarkable; the main reason is that, due to the extremely high molecular weight, there is a relatively small amount of crystal imperfections by chain ends.
While studying the fiber morphology it appeared that the initial "shish-kebab"-like structure [29] had changed to a very smooth fiber morphology after the hot-drawing stage.

2.8 *Gel spinning*

This process overlaps the technique, as described above, to a certain extent: especially the improvement by hot-drawing a surface-grown ultra-high molecular weight polyethylene (UHMWPE) fiber [25,27,28] is actually a gel spinning operation.
Gel spinning is applied to UHMWPE-fibers, spun from solution, that contain a large amount of solvent. By stretching the gelatic fiber under simultanuous evaporation of the solvent a highly oriented structure is formed. Factors that have proven to influence the mechanical properties [30] are (among others): the nature of the solvent, the initial polymer concentration (closely related to the initial amount of entanglements), the spin oven temperature, and the ultimate draw ratio.
Draw ratio values of 1500 and fiber production speeds of 300 m/min can be reached; mechanical properties can go up to 150 GPa for the Young's modulus and up to 6 GPa for the tensile strength.

3 Description and analysis of the process: orientation-induced crystallization in two-phase polymer flow

3.1 *Introduction*

As described before, there are many methods to obtain a high degree of orientation in flexible-chain macromolecules. A number of them (e.g. solid state extrusion and hydrostatic extrusion) are based on the observations as reported by Van der Vegt and Smit in 1967 [31]:
On extrusion of a crystallizable polymer melt through a converging die just above the melting temperarure of that polymer, under specific shear rate conditions the observed pressure rises dramatically until ultimately the flow stops; the melt has turned into a solid plug, thereby blocking the capillary entrance and thus preventing further flow. An example of the calculated apparent viscosity as a function of shear rate for polypropylene at different temperatures is given in fig. 3.1; the flowing polymer clearly no longer follows the "normal" power law shear thinning behaviour, but the viscosity appears to rise as a function of shear rate but also as a function of time, until ultimately the extrusion experiment has to be stopped.
Van der Vegt and Smit [31] explain this observation as being a result of the onset of crystallization in the flowing polymer melt due to a high degree of orientation caused by the elongational flow in the conical entrance to the capillary (similar to that by which the orientation causes spontaneous crystallization in a highly stretched rubber vulcanisate). The so-formed crystal seeds might act as crosslinks by incorporating several polymer chains into one tiny crystal, thus causing the apparent viscosity to increase dramatically.
An analysis of the solid material as formed under the conditions described above, shows very interesting mechanical properties: its stiffness (Young's modulus) and tensile strength are much higher than in the case of conventionally extruded material.
Further analysis also shows that there is a predominant orientation of the macromolecular chains in the extrusion direction; it appears that under the condition of strong elongational flow a more or less uniaxial alignment of the flexible polymer backbone chains is induced.

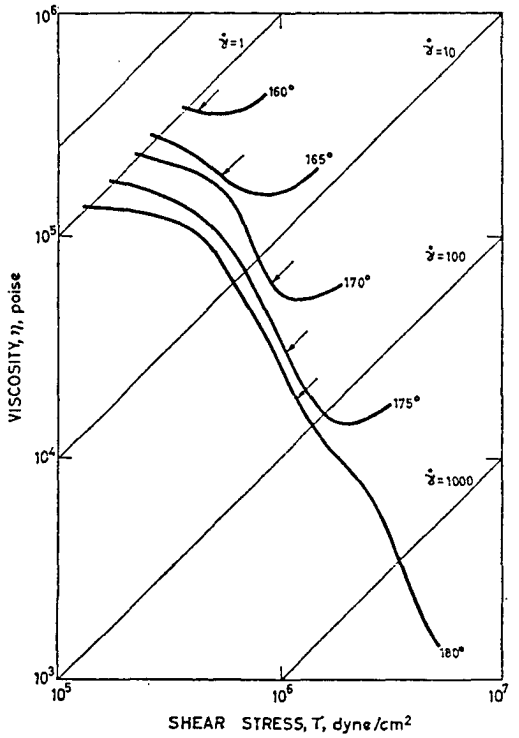


Fig.3.1 Apparent viscosity of Polypropylene as a function of shear stress at different temperatures.

As a result of this orientation the material crystallizes spontaneously in a so-called Extended-Chain Crystal (ECC) morphology; this structure is, as can be understood from the discussion in chapter 2, directly responsible for the remarkable mechanical properties. The high degree of molecular orientation is clearly depicted by the Wide Angle X-ray Scattering (WAXS) diffraction patterns as presented by Van der Vegt and Smit [31]: the normally circular diffraction rings (i.e. in the case of purely random and isotropic crystallization) are deformed to a pattern that is usually observed in the case of orientation inside the crystal lattice.

The melting point of this ECC-structure can, depending on the nature of the material under consideration, be much higher than in the case of conventionally crystallized material (the so-called Folded-Chain

Crystal or FCC structure); for instance, the melting point of highly oriented polypropylene (PP) is shown to be 179°C while the normal melting point of PP is 160°C (being not the equilibrium melting points but determined, for instance, by DSC-analysis and therefore dependent on factors like lamellar thickness and superheatability [32]). A schematic representation of both the FCC and the ECC crystal morphologies is given in figure 3.2.

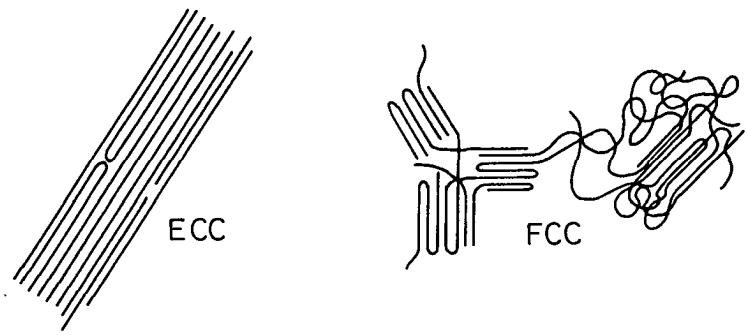


Fig.3.2 Schematic representation of Extended-Chain Crystal (ECC) and Folded-Chain Crystal (FCC) configuration.

This difference in melting point of the two crystal morphologies is directly responsible for the spontaneous crystallization; a polymer melt just above the melting point of the FCC-morphology is in fact undercooled with regard to the ECC-morphology. Once the molecules in the melt are stretched and their alignment gives rise to an ordering simular to that of the ECC-structure, crystallization will therefore occur spontaneously.

A related observation is reported by Odell et.al. [33]; they prepared high modulus (up to 100 GPa) strands of polyethylene by the controlled crystallization of lamellar overgrowths onto a small quantity of preformed flow-induced microfibrils in a capillary rheometer. The controlled overgrowth is induced by blocking the capillary exit and applying an increasing controlled hydrostatic pressure to the system. The flow-induced fibrils, assumed to contain the high molecular weight

fraction of the material, act as nuclei for this subsequent crystallization.
In this case the high modulus is not caused by a high degree of chain extension, but by the formation of tapering interlocking lamellar overgrowths; the overgrowth is forced to take place in a confined space.

3.2 *Process options*

The method as described in this thesis, is (like the methods mentioned at the beginning of this chapter) an effort to achieve materials with interesting mechanical properties by inducing a high degree of orientation in the crystal morphology in a continuous process. The basic concept is that the polymer melt, intrinsically showing the capacities as described above, is surrounded by a melt of another polymer that will not crystallize under the specific critical conditions. Consequently, this may either be an amorphous material or a semi-crystalline polymer, respectively with a lower glass transition temperature or melting point than the melting point of the material under consideration. The second polymer, obviously remaining fluid inside the specified, narrow range of extrusion conditions, should take care of the transport of the first polymer through the extrusion die during and after crystallization.
This principle can be looked upon in two essentially different ways:

1. The polymer of interest is dispersed in the second material; or
2. The first material forms a continuous concentric core within the other polymer.

The first route will ultimately lead to the formation of a self-reinforced polymer blend; the matrix material is filled with fibers that consist of highly oriented crystalline structures. Due to this oriented crystal morphology (in the ideal case: Extended Chain Crystals, or ECC) the melting point of these fibers is considerably higher than that of the same material under non-orientation conditions. This allows processing (e.g. injection moulding) of this special composite just under the elevated melting temperature of the dispersed phase, and consequently these very strong and stiff fibers

will reinforce the resulting product essentially like in the case of glass fibers.
In addition to that, the specific weight of polymer-reinforced polymers is lower than that of the corresponding glass-reinforced material, processing of these composites will not provide problems like they are often encountered in the case of glass fiber containing composites (equipment damage, environmental problems caused by glass dust, etc), and recycling of scrap and waste material seems to have a better perspective.
The second route will yield a continuous strand of high stiffness and high strength material within a skin of another polymer. The dimensions of this high-performance product can be influenced by changing the process geometry, and unlike in the case of fiber spinning, products of considerable proportions can be manufactured without recombining subassemblies. Like in fiber spinning the product will be of a continuous nature.
If there is no adhesion at all between the core and the skin material, the latter might be peeled off and recycled in the extrusion process. On the other hand, in the case of full adhesion, the skin material can provide an added value to the coextrusion product; factors like easy handling, adhesion to other materials, appearance, etc., can be enhanced by selecting the proper coextrusion partner.
It should be stressed, that shear flow is also capable of inducing a high degree of orientation in a polymer melt; however the polymer, when passing through a conical entrance, is assumed to undergo a much larger elastic deformation than when it flows through a capillary.

3.3 *Analysis of the process*

As an attempt to find a quantitative description of the phenomena of orientation-induced crystallization in a stretched polymer melt, this process is analysed in terms of a delicate balance between three time scales [34]:
1. The time scale of the experiment, τ_e;
2. The relaxation time, τ_r; and
3. The crystallization time, τ_c.

A short description and interpretation of these time scales will be given below.

3.3.1 *The time scale of the experiment*

This time scale represents the time during which the two-phase stretching experiment takes place; process parameters like extrusion die geometry, extrusion speed (and consequently the rate of elongation), and polymer combination can be varied to influence this time scale.
A lot of work has been done on two-phase flow through cylindrical dies; under a number of assumptions (stationary, isothermal, laminar flow, no slip at the wall, simple model fluids) the resulting models can describe the practical situation to a fair extent. However, two-phase polymer flow through a converging duct is a far more complicated matter; only a few considerations based on model descriptions of multi-layer polymer flow through a converging slit are known. A more detailed overview of two-phase flow through different geometries is given in section 4.1.

3.3.2 *The relaxation time scale*

It might be needless to say that the time scale balance considerations as presented in this thesis are principally applicable to flexible-chain macromolecules. This "restriction" directly implies that these polymeric molecules intrinsically exhibit a relaxation behaviour on a molecular scale during and directly after any magnitude and fashion of deformation.
This observation seems, at first sight, to be a bit trivial; however, the molecular relaxation plays a predominant role in the process of orientation-induced crystallization. Let us, as an example, consider the situation where the relaxation is faster than the deformation, or in other words, where the relaxation time scale is shorter than the time scale of the experiment. This situation can also be expressed in terms of the dimensionless Deborah number, defined as the ratio of the relaxation time and the observation time (in this case, τ_r/τ_e as

mentioned above). If the Deborah number is small ($\tau_r << \tau_e$); any induced orientation will relax immediately and the viscous contribution to the deformation will play a more important role than the elastic part, and no interesting results whatsoever are obtained.
On the other hand, if the Deborah number is large ($\tau_r >> \tau_e$), the deformation will be mainly elastic and a high degree of orientation can be obtained.
The latter is the more desirable situation; this also is the moment where the balance with the crystallization time scale has to be taken into account. A separate treatment of this topic will be given below.
From the arguments as presented above, one can clearly conclude that knowledge of the relaxation behaviour of a stretched crystallizable polymer melt is of the greatest importance for the ability to realize the principle of orientation-induced crystallization in a two-phase flow as a continuous process. A combined experimental and theoretical study on this relaxation behaviour is given in chapter 5.

3.3.3 *The crystallization time scale*

As already mentioned above, in the situation where a considerable degree of orientation can be induced in a crystallizable polymer melt, the crystallization kinetics will start to play an important role. This can also be interpreted in terms of a delicate time scale balance: again, if one is able to achieve a sufficient degree of orientation during elongational flow of a crystallizable polymer melt, the crystallization should on one hand not be too fast; the obtained orientation will be frozen in before an optimum is reached, and also there is a risk of blockage in the extrusion die by the formation of a solid plug with larger dimensions than the ultimate extrusion aperture.
On the other hand, if the crystallization is too slow, the obtained orientation will relax away before it is fixed in a crystal morphology and the resulting product, although easily manufactured, will not exhibit the desired properties.
It can be concluded that the crystallization kinetics of polymer melts stretched in elongational flow is of essential importance; also

scientists, working in the field of injection molding of crystallizable polymer compounds, are eager to obtain acquaintance with this subject. However to my knowledge, no totally satisfying method to study this phenomenon has been developed until now.
Purely qualitatively something can be said about the enhancement of polymer crystallization in elongational flow in the presence of a stationary seed. First of all it should be emphasised that this phenomenon has already been observed in dilute solutions of ultra-high molecular weight polyethylene (UHMWPE) in xylene or decaline, for instance by Pennings and Zwijnenburg ([22,23], see also section 2.7). Indications for a possible application of exactly the same principle to crystallizable polymer melts are clearly given by Sakellarides and McHugh [35-37]: subsequent extrusion of pure high-density polyethylene (HDPE) followed by pure linear low-density polyethylene (LLDPE) through a tapered die, mounted with a row of five stainless steel needles, forces the remaining amount of HDPE to flow past the needles and to undergo orientation, producing fibrous crystals. After some time however, all the HDPE is consumed and the extrudate contains LLDPE only. A similar experiment, using a blend containing 30 percent HDPE and 70 percent LLDPE, did also produce bundle-like fibrous structures but not as perfectly positioned along the central axis of the extrudate as the fibers produced by the successive extrusions.
These results clearly show that a continuous extrusion of oriented fibers, using needle-like structures as seed sites for enhanced orientation, is feasible. Later more attention will be given to this principle.

As a conclusion from the arguments mentioned in this chapter, the decision to study deformation, relaxation and crystallization phenomena in two-phase polymer melt flow appears to be justified. Of course, a practical application should always be the primary goal, but a better understanding of the theoretical backgrounds of the process in question might lead to more appropriate experimental work.

4 Deformational behaviour of two-phase molten polymer systems

4.1 *Introduction*

When one wants to examine the effects that play a predominant role in the deformation of molten polymer blends, a good definition of this two-phase system is required.
First of all the two polymers in every system are assumed to be incompatible, meaning they cannot be mixed on a molecular scale or, to put it in other terms, the two materials have a finite interfacial tension.
In the scope of this thesis two systems have to be taken into account:
a) Concentric cocontinuous systems and
b) Dispersed systems.

Ad. a) By concentric cocontinous systems are meant those systems where one material forms a continuous cylindrical core within a concentric shell of the other material.
Ad. b) By dispersed systems are meant those systems where one material forms a continuous phase and where the other material is more or less finely dispersed in spherical droplets.

The deformation behaviour of both systems in a well-defined flow field has to be known to a certain extent in order to allow us to understand this behaviour in relation to the relaxation behaviour; a careful balance between these two phenomena always plays a predominant role in the process of self-reinforcement of polymer blends by orientation-induced crystallization (see section 3.3).
In this chapter only uniaxial flow will be considered; the reason for this choice is obviously the geometry that is usually chosen for the experimental work (cylindrical channels and conical dies).

4.2 *Cocontinuous two-phase systems*

Cocontinuous flow of two non-Newtonian fluids through a tapered entrance to a capillary is a complicated subject; specific problems

might be solved with the aid of finite elements methods, but general analytical modelling is impossible.
Therefore, in the framework of this study only the flow of the concentric cocontinuous system through the capillary after the conical entrance has been taken into consideration. This part of the problem can easily be solved analytically, and furthermore we were able to observe the development of the flow in this region experimentally. A detailed description of these experiments and a comparison of the results with theoretical predictions will be given later on in this chapter.

For the description of two-phase concentric and cocontinuous flow through a cylindrical channel the following assumptions were made:

a) The temperature is constant throughout the whole geometry, which implies no temperature influence on the viscosities of both fluids;
b) Once the flow is fully developed the pressure gradients are constant;
c) Both materials match the same fluid-mechanical model.

The models, taken into consideration, are:

a) Newtonian: $\tau_s = -\eta\ \dot{\gamma}$; (1)

b) Second order: $\underline{\tau} = -\alpha_1\ \underline{\dot{\gamma}} + \alpha_2\ \frac{D}{Dt}\ \underline{\dot{\gamma}} - \alpha_{11}\ \{\underline{\dot{\gamma}} \cdot \underline{\dot{\gamma}}\}$; (2)

c) Power law: $\tau_s = -K\ \dot{\gamma}^n$. (3)

4.2.1 *Newtonian fluids*

Let us consider two Newtonian fluids flowing concentrically through a cylindrical channel. The variables used in the following equations are more or less defined in figure 4.1.
Written in cylindrical coordinates the equation of motion in the x-direction reads [38]

$$\rho \left(\frac{\partial v_x}{\partial t} + v_r \frac{\partial v_r}{\partial r} + \frac{v_\theta}{r} \frac{\partial v_x}{\partial \theta} + v_x \frac{\partial v_x}{\partial x} \right) =$$

$$- \left(\frac{1}{r} \frac{\partial}{\partial r} (r \tau_{rx}) + \frac{1}{r} \frac{\partial \tau_{\theta x}}{\partial \theta} + \frac{\partial \tau_{xx}}{\partial x} \right) - \frac{\partial P}{\partial x} + \rho g_x \qquad (4)$$

where ρ = the density of the fluid
v = the velocity of the fluid
τ = the shear stress
P = the isotropic pressure
g = the gravitational acceleration
r,x as defined in figure 4.1.

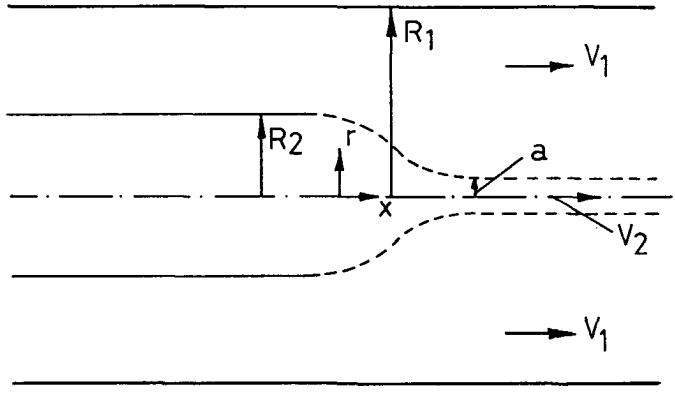


Fig.4.1 Representation of two-phase concentric flow through a cylindrical channel. R_1 = radius of cylinder, R_2 = radius of inner cylinder, a = radius core material, v = velocity, r,x = coordinates.

In our specific case this equation can be simplified for the following reasons:

1) We are considering stationary flow, so $\frac{\partial}{\partial t} = 0$.
2) There is only flow in the x-direction, so $v_\theta = v_r = 0$ and consequently $\tau_{\theta x} = \tau_{xx} = 0$.
3) There are no velocity fluctuations over the length of the geometry, so $\frac{\partial v_x}{\partial x} = 0$.
4) Gravitational forces play no role, so $g_x = 0$.

This leaves us with the following equation:

$$\frac{1}{r}\frac{\partial}{\partial r}(r\,\tau_{rx}) = -\frac{dP}{dx} \tag{5}$$

After substitution of the Newtonian equation

$$\tau_{rx} = -\eta\frac{dv}{dr} \tag{6}$$

we arrive at the following set of equations:

$$v_2(r) = \frac{1}{4}\left(-\frac{dP}{dx}\right)\left(\frac{1}{\eta_2}(a^2 - r^2) + \frac{1}{\eta_1}(R_1^2 - a^2)\right) \tag{7}$$

$$v_1(r) = \frac{1}{4}\left(-\frac{dP}{dx}\right)\left(\frac{1}{\eta_1}(R_1^2 - r^2)\right) \tag{8}$$

$$\phi_2 = \frac{\pi}{8}\left(-\frac{dP}{dx}\right)\left(\frac{1}{\eta_2}a^4 + \frac{2}{\eta_1}a^2(R_1^2 - a^2)\right) \tag{9}$$

$$\phi_1 = \frac{\pi}{8}\left(-\frac{dP}{dx}\right)\left(\frac{1}{\eta_1}(R_1^2 - a^2)^2\right) \tag{10}$$

where v_1 = the velocity of the matrix material
v_2 = the velocity of the core material
ϕ_1 = the volume flux of the matrix material
ϕ_2 = the volume flux of the core material
η_1 = the viscosity of the matrix material
η_2 = the viscosity of the core material
P = the isotropic pressure
a, r, R_1 as defined in figure 4.1.

The radius of the core material can now be calculated by dividing equation (9) by equation (10). This results in

$$\frac{\phi_2}{\phi_1} = \frac{\frac{\eta_1}{\eta_2}\frac{a^4}{R_1^4} + 2\frac{a^2}{R_1^2}\left(1 - \frac{a^2}{R_1^2}\right)}{\left(1 - \frac{a^2}{R_1^2}\right)^2} \tag{11}$$

Or with $\lambda = a/R_1$:

$$\frac{\phi_2}{\phi_1}(1-\lambda^2)^2 = \frac{\eta_1}{\eta_2}\lambda^4 + 2\lambda^2 - 2\lambda^4 \qquad (12)$$

Equation (12) can be rewritten as

$$\lambda^4\left(\frac{\phi_2}{\phi_1} - \frac{\eta_1}{\eta_2} + 2\right) + \lambda^2\left(-2\frac{\phi_2}{\phi_1} - 2\right) + \frac{\phi_2}{\phi_1} = 0 \qquad (13)$$

This is a quadratic equation in λ^2 and can be solved as

$$\lambda^2 = \frac{\frac{\phi_2}{\phi_1} + 1 - \sqrt{\frac{\phi_2}{\phi_1}\frac{\eta_1}{\eta_2} + 1}}{\frac{\phi_2}{\phi_1} - \frac{\eta_1}{\eta_2} + 2} \qquad (14)$$

for $\frac{\phi_2}{\phi_1} \neq \frac{\eta_1}{\eta_2} - 2$; if $\frac{\phi_2}{\phi_1} = \frac{\eta_1}{\eta_2} - 2$, λ^2 can be directly calculated from equation (13).

So if the volume fluxes and the viscosities of both components are given, on the basis of this purely Newtonian model the diameter of the core material in relation to the total diameter of the geometry can be calculated.

4.2.2 *Second order fluids*

Second order fluids are defined as those fluids which have a constant viscosity and which exhibit a quadratic dependance of the first and second normal stress differences on the shear rate $\dot{\gamma}$. The basic equation for a second order fluid model in shear flow is given by:

$$\underline{\tau} = -\alpha_1 \underline{\dot{\gamma}} + \alpha_2 \frac{D}{Dt}\underline{\dot{\gamma}} - \alpha_{11}\{\underline{\dot{\gamma}} \cdot \underline{\dot{\gamma}}\} \qquad (2)$$

where $\alpha_1 = \eta$ = the apparent viscosity

$\alpha_2 = \frac{1}{2}\Psi_1$

$\alpha_{11} = \frac{1}{2}\Psi_1 + \Psi_2$

Ψ_1 = the first normal stress difference coefficient

Ψ_2 = the second normal stress difference coefficient

If $\frac{D}{Dt}\underline{\dot{\gamma}}$ is taken as the corotational derivative, the following relations are valid:

$$\frac{D}{Dt}\,\underline{\dot{\gamma}} = \frac{\partial}{\partial t}\,\underline{\dot{\gamma}} + \{\underline{v}\cdot\nabla\underline{\dot{\gamma}}\} + \tfrac{1}{2}\,(\{\underline{\underline{\omega}}\cdot\underline{\dot{\gamma}}\} - \{\underline{\dot{\gamma}}\cdot\underline{\underline{\omega}}\}) \qquad (15)$$

with $\underline{\dot{\gamma}} = [\nabla\,\underline{v} + \nabla\,\underline{v}^T]$ and $\underline{\underline{\omega}} = [\nabla\,\underline{v} - \nabla\,\underline{v}^T]$.

Again in this case, we write the equation of motion in the x-direction in cylindrical coordinates, and as in the case of Newtonian fluids the equation can be simplified:

1) We are considering stationary flow, so $\frac{\partial}{\partial t} = 0$.
2) There is only flow in the x-direction, so $v_\theta = v_r = 0$.
3) No velocity changes over the length of the cylindrical geometry, so $\frac{\partial v_x}{\partial x} = 0$.
4) Gravitational forces play no role, so $g_x = 0$.

The tensors used in the equations, are represented by

$$\underline{\dot{\gamma}} = \begin{bmatrix} 0 & (\frac{\partial v_x}{\partial r}) & 0 \\ (\frac{\partial v_x}{\partial r}) & 0 & 0 \\ 0 & 0 & 0 \end{bmatrix} \qquad \underline{\underline{\omega}} = \begin{bmatrix} 0 & -(\frac{\partial v_x}{\partial r}) & 0 \\ (\frac{\partial v_x}{\partial r}) & 0 & 0 \\ 0 & 0 & 0 \end{bmatrix}$$

$$\{\underline{\dot{\gamma}}\cdot\underline{\dot{\gamma}}\} = \begin{bmatrix} (\frac{\partial v_x}{\partial r})^2 & 0 & 0 \\ 0 & (\frac{\partial v_x}{\partial r})^2 & 0 \\ 0 & 0 & 0 \end{bmatrix} \qquad \{\underline{\underline{\omega}}\cdot\underline{\dot{\gamma}}\} = \begin{bmatrix} -(\frac{\partial v_x}{\partial r})^2 & 0 & 0 \\ 0 & (\frac{\partial v_x}{\partial r})^2 & 0 \\ 0 & 0 & 0 \end{bmatrix}$$

$$\{\underline{\dot{\gamma}}\cdot\underline{\underline{\omega}}\} = \begin{bmatrix} (\frac{\partial v_x}{\partial r})^2 & 0 & 0 \\ 0 & -(\frac{\partial v_x}{\partial r})^2 & 0 \\ 0 & 0 & 0 \end{bmatrix} \qquad \{\underline{v}\cdot\nabla\underline{\dot{\gamma}}\} = \underline{\underline{0}}$$

Substitution of these tensors in the basic equation for second order fluids yields the following stress tensor:

$$\underline{\tau} = \begin{bmatrix} -(\Psi_1+\Psi_2)\dot{\gamma}^2 & -\eta\dot{\gamma} & 0 \\ -\eta\dot{\gamma} & -\Psi_2\dot{\gamma}^2 & 0 \\ 0 & 0 & 0 \end{bmatrix}$$

The relevant terms are substituted in the equation of motion, yielding

$$(\frac{\partial v_x}{\partial r})^2 = \frac{P(x)}{\Psi_2} \tag{16}$$

$$r(\frac{\partial v_x}{\partial r}) = \frac{\partial P}{\partial x}\frac{r^2}{2\eta} \tag{17}$$

The second equation leaves us with essentially the same solution as in the case of two Newtonian fluids; equation (17) is identical to equation (5) combined with equation (6). From this calculation result we can conclude that in the case of second order fluids elastic effects have no influence on the velocity profile, and consequently on the diameter ratio of the type of flow as considered here.

4.2.3 *Power law fluids*

Concentric cocontinuous flow of power law fluids for which holds

$$\tau_s = -K\,\dot{\gamma}^n \tag{3}$$

has already been treated extensively by Han [39]. From these calculations, we can take the equations for the velocities of both fluids under steady state conditions:

$$v_1 = (-\frac{1}{2K_1}\frac{dP}{dx})^{\alpha_1}\cdot\frac{1}{\alpha_1+1}\,(R_1^{\alpha_1+1} - r^{\alpha_1+1}) \tag{18}$$

$$v_2 = (-\frac{1}{2K_2}\frac{dP}{dx})^{\alpha_2}\cdot\frac{1}{\alpha_2+1}\,(a^{\alpha_2+1} - r^{\alpha_2+1}) + (-\frac{1}{2K_1}\frac{dP}{dx})^{\alpha_1}\cdot\frac{1}{\alpha_1+1}\,(R_1^{\alpha_1+1} - a^{\alpha_1+1}) \tag{19}$$

where $\alpha_1 = 1/n_1$

$\alpha_2 = 1/n_2$

n_1, n_2 = the power law indexes of the matrix and core fluid

K_1, K_2 = the power law constants of the matrix and core fluid, respectively.

R_1, r, a as defined in figure 4.1.

From these equations we can derive the volume fluxes:

$$\phi_1 = 2\pi \int_0^{R_1} r\, v_1\, dr =$$

$$= \frac{2\pi}{\alpha_1+1} \left(-\frac{1}{2K_1} \frac{dP}{dx}\right)^{\alpha_1} \cdot \left(\tfrac{1}{2}\left(R_1^{\alpha_1+3} - R_1^{\alpha_1+1} a^2\right) + \frac{1}{\alpha_1+3} \left(a^{\alpha_1+3} - R_1^{\alpha_1+3}\right)\right) \quad (20)$$

$$\phi_2 = 2\pi \int_0^{a} r\, v_2\, dr = \frac{\pi}{\alpha_2+3} \left(-\frac{1}{2K_2} \frac{dP}{dx}\right)^{\alpha_2} \cdot a^{\alpha_2+3} +$$

$$\frac{\pi}{\alpha_1+1} \left(-\frac{1}{2K_1} \frac{dP}{dx}\right)^{\alpha_1} \cdot \left(R_1^{\alpha_1+1} a^2 - a^{\alpha_1+3}\right) \quad (21)$$

We can take ϕ_1/ϕ, where $\phi = \phi_1 + \phi_2$, to calculate the steady state diameter of the core material (parameter a in figure 4.1). This results in

$$\frac{\phi_1}{\phi} = \frac{\left(-\frac{R_1}{2K_1} \frac{dP}{dx}\right)^{\alpha_1} \frac{R_1^3}{\alpha_1+3} \left(1 - \frac{\alpha_1+3}{\alpha_1+1} \lambda^2 + \frac{2}{\alpha_1+1} \lambda^{\alpha_1+3}\right)}{\left(-\frac{R_1}{2K_2} \frac{dP}{dx}\right)^{\alpha_2} \frac{R_1^3}{\alpha_2+3} \lambda^{\alpha_2+3} + \left(-\frac{R_1}{2K_1} \frac{dP}{dx}\right)^{\alpha_1} \frac{R_1^3}{\alpha_1+3} \left(1-\lambda^{\alpha_1+3}\right)} \quad (22)$$

where $\lambda = a/R_1$.

In combination with equation (20) it can be shown that the following relation is valid:

$$\frac{\phi_1}{\phi} \lambda^{\alpha_2+3} \frac{\alpha_1+3}{\alpha_2+3} \left(\frac{K_1}{K_2}\right)^{\alpha_2} \left(\frac{\phi_1}{1 - \frac{\alpha_1+3}{\alpha_1+1} \lambda^2 + \frac{2}{\alpha_1+1} \lambda^{\alpha_1+3}} \frac{\alpha_1+3}{\pi R_1^3}\right)^{\frac{\alpha_2-\alpha_1}{\alpha_1}} =$$

$$\lambda^{\alpha_1+3} \left(\frac{\phi_1}{\phi} + \frac{2}{\alpha_1+1}\right) + \lambda^2 \left(\frac{\alpha_1+3}{\alpha_1+1}\right) - \left(1 - \frac{\phi_1}{\phi}\right) = 0 \quad (23)$$

Substitution of $\alpha_1 = \alpha_2 = 1$, $\frac{K_1}{K_2} = \frac{\eta_1}{\eta_2}$ and $\phi = \phi_1 + \phi_2$ in equation (23) should result in the Newtonian solution; indeed, rewriting in a quadratic form yields equation (14).
Solutions to equation (23) can be found numerically.

4.3 *Experimental observations of the coextrusion diameter ratio*

4.3.1 *Equipment*

In order to study the coextrusion process a special experimental set-up was built, consisting of two extruders mounted to a coextrusion die, the construction of which is shown in figure 4.2. It takes care of the formation of concentric cocontinuous two-phase polymer flow. Onto this coextrusion head a number of different dies can be mounted.

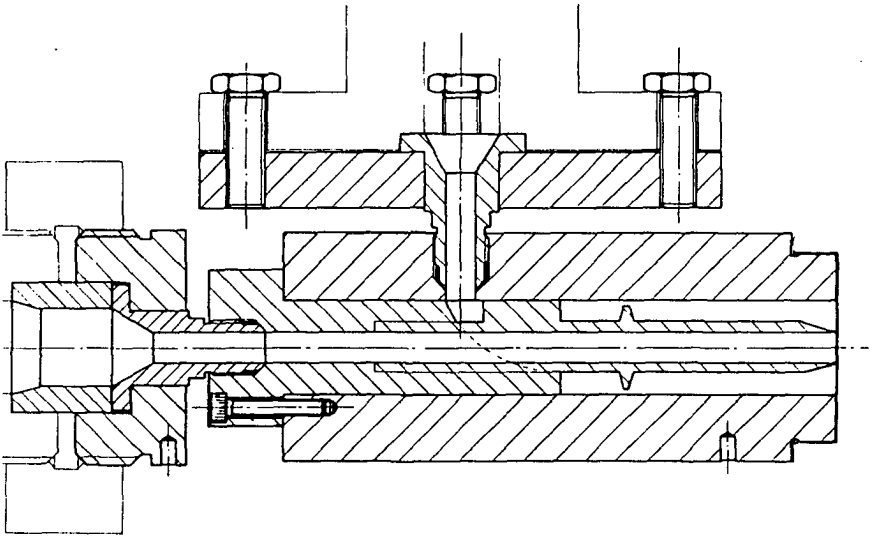


Fig.4.2 Construction of the coextrusion die.

For the purpose of studying the settlement of the flow in the capillary as well as other phenomena such as deformational behaviour in the conical entrance and process stability, a set of two separate dies was constructed in which glass windows, incorporating the conical entrance (or part of it) and part of the capillary, could be mounted. A schematical drawing of these dies is shown in figure 4.3.

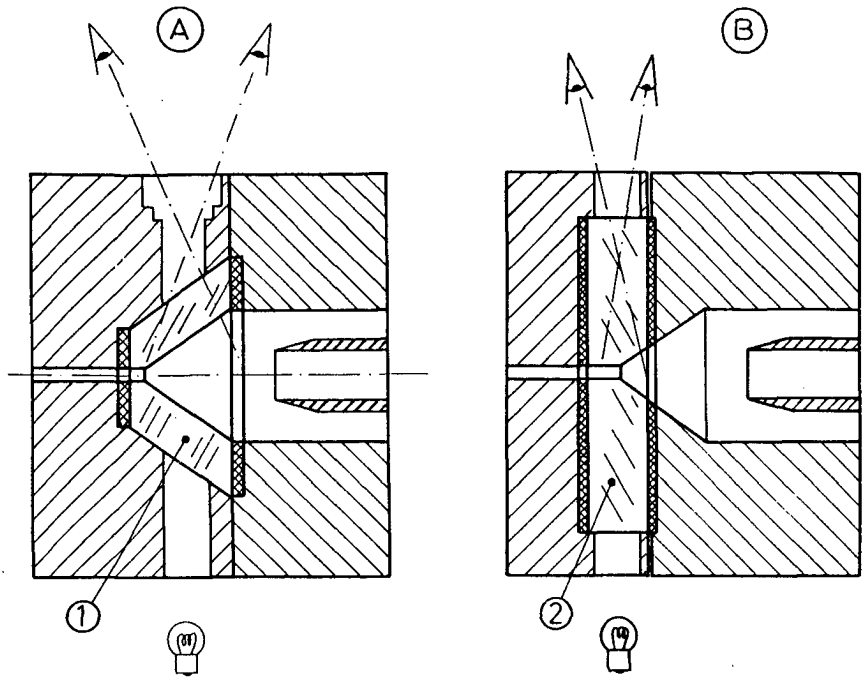


Fig.4.3 Schematical representation of the dies for visual observation; a: the complete conical entrance made out of glass (1), b: the last part of the entrance in glass (2).

The glass windows are made out of Zerodur glass (Schott); this brand of glass has been developed in space technology and has no measurable coefficient of expansion. Therefore it does not crack due to internal stresses developed by the periodical heating up and cooling down of the equipment.

The window as shown in figure 4.3a gives the broadest field of view; however, due to the large area on which the isotropic melt pressure acts, this window can only withstand pressures up to 25 MPa. Under those conditions where substantially higher pressures could be expected, the die shown in figure 4.3b had to be used. In any case the diameter ratio (meaning the ratio of the diameter of the core melt and the capillary) after settlement of the flow in the capillary could be observed by means of video equipment.

With this equipment a series of experiments was performed using

different materials (thereby varying the viscosities of both components) and different extruder screw speeds (thereby varying the volume fluxes).

4.3.2 *Materials*

For the coextrusion experiments where the aim was to determine the diameter ratio of the concentric flow in the capillary after the conical entrance, in all cases polypropylene was used for the core material and polystyrene for the matrix material. The power law indexes and constants were calculated from results of flow curve measurements on a capillary rheometer; the average value of the indexes was used for the model calculations. An overview of the grades that were used together with their power law parameters (n and K in equation (3)) is given in table 4.4.

Polypropylene: Carlona P (Shell) Grade	Power law parameters Index n (average)	Constant K ($Ns^n m^2$)
F 6100	0.34	$2.75 \cdot 10^4$
G 6100	0.34	$2.57 \cdot 10^4$
J 6100	0.34	$1.78 \cdot 10^4$
K 6100	0.34	$1.26 \cdot 10^4$
L 6100	0.34	$1.17 \cdot 10^4$
P 6100	0.34	$1.12 \cdot 10^4$
S 6100	0.34	$0.76 \cdot 10^4$
Polystyrene: Hostyren (Hoechst) Grade	**Power law parameters Index n (average)**	**Constant K ($Ns^n m^2$)**
N 5000	0.28	$4.47 \cdot 10^4$
N 4000	0.28	$2.88 \cdot 10^4$
N 3000	0.28	$2.19 \cdot 10^4$
N 2000	0.28	$1.38 \cdot 10^4$

Table 4.4 Grades of polypropylene and polystyrene used in the coextrusion experiments with their power law parameters.

4.3.3 *Results*

Not every polymer combination that can be taken from table 4.4 is suitable for performing coextrusion experiments with the aid of the equipment as described in section 4.3.1. In the case of a core material viscosity much lower than the matrix material viscosity a spiral shaped distortion of the concentric flow was detected both by monitoring the glass conical entrance and capillary during flow and by analysing the extrudate. Moreover, the core material showed a tendency to flow along the capillary wall, thus reversing the concentric system. This observation is in agreement with descriptions by Maclean [40] and Everage [41] based on a minimum energy dissipation theory.
To avoid these instability problems, only experiments with combinations of the following polymers were performed:

Hostyren N 2000 and N 3000 (matrix material);
Carlona P G 6100, J 6100, L 6100 and S 6100 (core material).

With each combination of these materials, the following volume fluxes were used:

ϕ_{core} = 9.3 cm^3/min and ϕ_{matrix} = 18.6 cm^3/min;
ϕ_{core} = 9.0 cm^3/min and ϕ_{matrix} = 37.8 cm^3/min;
ϕ_{core} = 8.4 cm^3/min and ϕ_{matrix} = 57.0 cm^3/min.

With every polymer and flux combination the diameter of the core material was measured; the diameter of the capillary itself was known to be 3.0 mm, so this value was used to calibrate the video tape recordings of the concentric flow in the capillary. All measurements were performed at temperature control settings of 175°C.
Results of these measurements are shown in figure 4.5, where the diameter ratio $\lambda = a/R_1$ (see figure 4.1) is plotted against the logarithm of the ratio of the power law constants of both polymer melts. Together with the experimental points both the theoretical predictions from the power law model (equation (23)) and from the Newtonian model (equation (14)) are shown.

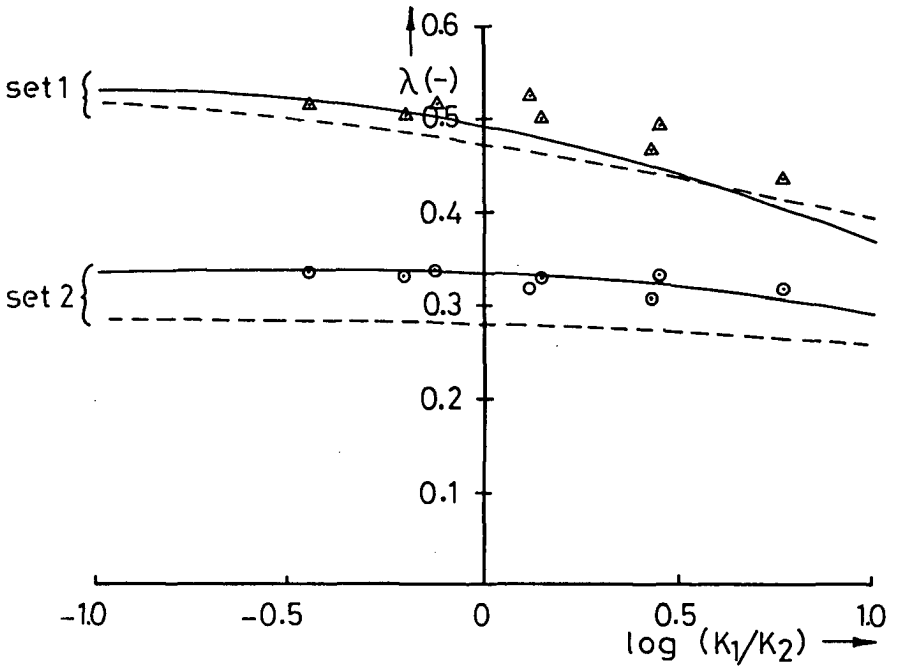


Fig.4.5 Experimental values and theoretical predictions of λ *(=* a/R_1*, see figure 4.1) plotted against the logarithmic ratio of the power law constants, log* (K_1/K_2)*. Polymer melt 1 = Hostyren, different grades; polymer melt 2 = Carlona P, different grades. Temperature = 175°C. Full line: power law model (equation (23)); power law parameters as mentioned in table 4.4. Dotted line: Newtonian model (equation (14)). Set 1:* $\phi_{matrix}/\phi_{total} = 0.67$*; set 2:* $\phi_{matrix}/\phi_{total} = 0.87$*.*

4.3.4 *Discussion*

From figure 4.5 it clearly follows that (as could be expected) the power law model is a better choice to describe concentric cocontinuous flow of two polymer melts than is the Newtonian model.
As already mentioned in section 4.2.2 in the case of second order fluids the introduction of elastic effects has no influence on the theoretical predictions, once steady flow is assumed.
Still there is some deviation in the regions of lower matrix volume

fluxes and consequently lower pressures. A possible explanation for this phenemenon might be the temperature and pressure dependence of the apparent melt viscosity: due to viscous heating the melt temperature is estimated to be about 10°C higher then the set value (estimation based on measurements with a thermocouple mounted perpendicular to the flow direction); furthermore, especially at lower volume fluxes the pressure is lower than the level at which the flow curves were measured. Consequently the apparent viscosity should be corrected for both temperature and pressure effects.
Unfortunately, in particular regarding the pressure dependence, in literature only little information can be found on this topic, although the general formula for the corresponding corrections is unanimously assumed to be

$$\eta = \eta^* \exp\left(\bar{\alpha}\,(T-T^*)\right) \exp\left(\bar{\beta}\,(p-p^*)\right) \qquad (24)$$

with $\bar{\alpha} = n\,\bar{\alpha}_0$ and $\bar{\beta} = n\,\bar{\beta}_0$
where η = the apparent viscosity
η^* = the viscosity, measured at temperature T^* and pressure p^*
T = the actual temperature
p = the actual pressure
$\bar{\alpha}_0$ = the temperature coefficient in the Newtonian region
$\bar{\beta}_0$ = the pressure coefficient in the Newtonian region
n = the power law index.

In his thesis Laven [42] mentions some values of $\bar{\alpha}$ and $\bar{\beta}$ for polystyrene but none for polypropylene, and no such values could be found elsewhere until now. Just to find out whether a correction for the pressure dependence of the apparent viscosity of only one phase might influence the theoretical predictions of the diameter ratio, based on the power law model, in the right direction, the viscosity of the polystyrene melt was recalculated using

$$\bar{\alpha} = \frac{\partial \ln \eta}{\partial T} = -1.76 \cdot 10^{-2}\ K^{-1} \text{ and}$$

$$\bar{\beta} = \frac{\partial \ln \eta}{\partial p} = 2.07 \cdot 10^{-8}\ Pa^{-1}$$

(values taken from Laven [42]).
Taking T = 185°C, p = 5 MPa, T^* = 175°C and p^* = 20 MPa (which are realistic values regarding the coextrusion process as studied here), the resulting theoretical predictions are shown in figure 4.6. On the basis of these results we can conclude that the correction, as used here, yields a noticeable improvement regarding the agreement between the power law predictions and the experiments, although the effect is not very large.

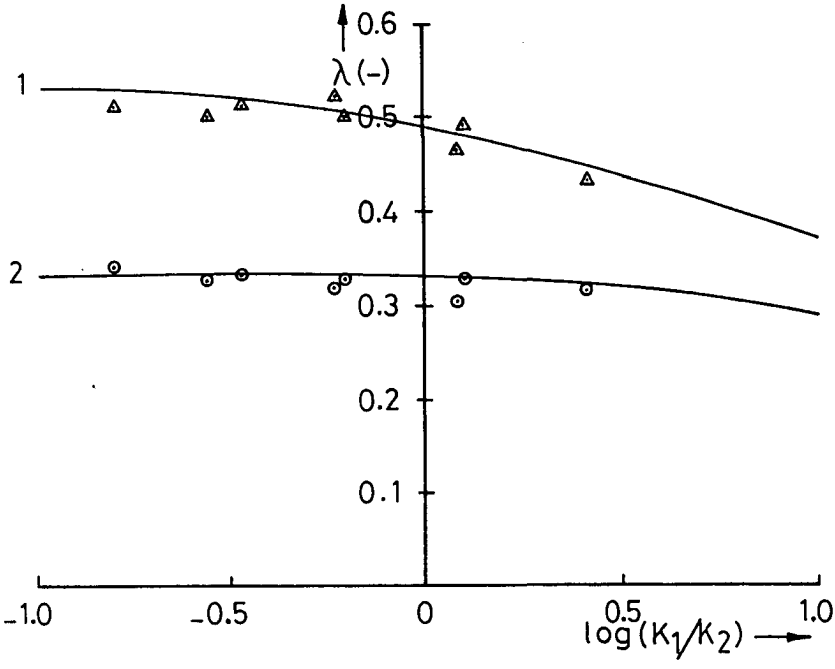


Fig.4.6 Experimental values and theoretical predictions of λ (= a/R_1, see figure 4.1) plotted against the logarithmic ratio of the power law constants, log (K_1/K_2). Polymer melt 1 = Hostyren, different grades; polymer melt 2 = Carlona P, different grades. Temperature = 175°C. Full line: power law model (equation (23)) with correction for temperature and pressure dependence of the viscosity of the polystyrene melt (melt 1); power law parameters as mentioned in table 4.4. Set 1: $\phi_{matrix}/\phi_{total} = 0.67$; set 2: $\phi_{matrix}/\phi_{total} = 0.87$.

4.4 *Dispersed two-phase systems*

4.4.1 *Introduction*

If one wants to treat deformation of dispersed two-phase molten polymer systems one immediately enters a wide region of scientific interest, namely the morphological and (micro)rheological aspects, as well as the relations between the two, of polymer blending processes.
In the scope of a general research program at the Laboratory of Polymer Technology of the Delft University of Technology the deformation and break-up of single droplets in different kinds of flows is studied with the aim to find a theoretical, or at least semi-empirical description of the micro-rheological behaviour that plays an important role in the formation of incompatible polymer blends.
Starting with model fluids which can be described with simple rheological models (Newtonian, power law, second order, Hookean), and the deformation and break-up behaviour of which can be studied at room temperature, many experiments have been and are still being performed to test the validity of the models that are commonly used.
In his thesis Elmendorp [43] has shown a number of phenomena that play an important role in morphology development during a polymer blending process: droplet deformation and break-up in different kinds of flows, break-up of fluid threads and coalescence of droplets.
Existing treatments of the deformation problem for Newtonian systems as proposed by Taylor [44] and Cox [45] can be extended to second order solutions [46], but this gives no improvement, thus indicating that the perturbation analysis as used in these treatments probably does not converge for this specific problem. This leaves us with a description of droplet deformation as a function of the microrheological parameters of the process that is only valid up to very small deformations.
The break-up criteria as formulated by Grace [47] and later confirmed for Newtonian systems by Bentley and Leal [48], are able to predict the critical Weber numbers (defined as $We = \eta_1 \dot{\gamma} R/\sigma$, where η_1 = the shear viscosity of the matrix phase, $\dot{\gamma}$ = the shear rate, R = the radius of the undeformed droplet and σ = the interfacial tension)

where break-up occurs. Van der Reijden-Stolk [49] has shown that, during a blending process, this allows prediction of a maximum droplet radius by only looking at the regions where the highest rates of deformation occur, provided we are dealing with a very dilute dispersion. In the case of higher concentrations coalescence of droplets will start to play an important role, resulting in a larger droplet size compared to the theoretical prediction.
In purely two-phase systems the polymer-polymer interfaces are clean and thus mobile, resulting in a high coalescence probability [43]; addition of copolymers that act as a surfactant, causes the interface to become immobile, hence lowering the coalescence probability and consequently yielding a finer dispersion.

4.4.2 *Fiber formation*

As already mentioned in section 3.2, the deformation of polymer dispersions might lead to the formation of fibers. If this fiber formation occurs in the critical region where orientation-induced crystallization can take place, extended-chain crystals can be formed, resulting in a substantially higher strength and stiffness of these fibers. Provided that there is enough adhesion between the two phases upon complete solidification this process will lead to the formation of a self-reinforced polymer blend.
Before even trying to realize this phenomenon in a continuous process, the conditions under which fiber formation takes place in a controlled, regular and reproducable way, have to be known and understood. A lot of work on this topic has been done by Vinogradov, Tsebrenko and coworkers [50,51,53-57,59]. These research workers also try to relate the phenomenon of fiber formation to the rheological properties of the individual components and of the blend under investigation. This approach gives access to an enormously broad field of research, both fundamental and phenomenological, the latter of which is particulary interesting in the scope of this work.
Assuming the usual incompatibility of polymers, Tsebrenko and coworkers [50,51] start by stating that as a result of a blending process radical changes in thermodynamical and physico-mechanical

properties, as well as in structure, are obtained. Therefore they conclude that blending of polymers is an efficient method to obtain materials with improved or totally different properties as compared to the starting materials. Fiber reinforcement of one phase in the bulk of the other polymer is just one example.

All methods to investigate fiber formation as described in literature, come down to one principle: the polymer dispersion is extruded through a converging entrance and a capillary. Leading scientists in this field like Tsebrenko, but also Narasaiah Alle and Lyngae-Jørgensen [52] unanimously assume, that fiber formation doesn't take place during flow in the capillary or afterwards but during flow through the converging entrance to the capillary. The driving forces in this process are the elongational stresses. A schematic representation of this fibrillation (the rheological parameters are not yet taken into account) is given in figure 4.7.

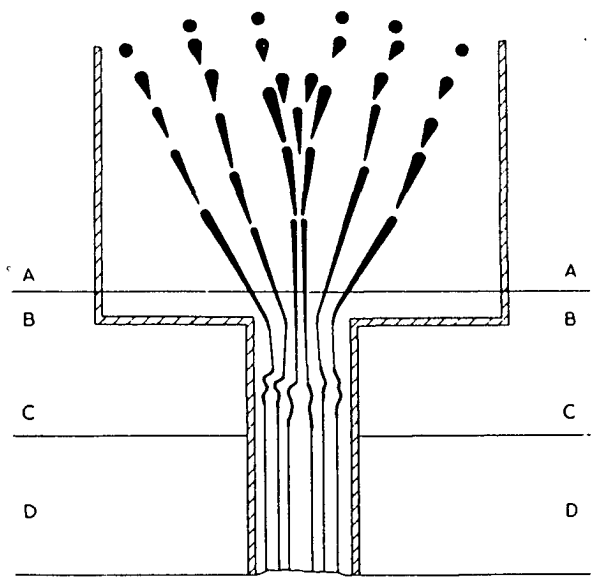


Fig.4.7 Schematic representation of the fibrillation process in the entrance zone and in the ducts.

A standard experiment can be represented as follows: The molten polymer mixture is extruded from the viscosimetric container through the appending capillary. As a result of the elongational stresses in the direction of flow the dispersed particles of the fiber-forming component stretch and coalesce in the entrance zone (A, figure 4.7). Close to the entrance to the capillary (B, figure 4.7) the flow suddenly contracts and shortly after that the flow undergoes the influence of the capillary wall, causing shearing and retardation of the flow (C, figure 4.7) which results in a local reduction and subsequent increase in the fiber diameter. Also the degree of parallel arrangement decreases locally; further on in the capillary, under the influence of the shearing forces, the joint parallel alignment of the fibers is re-established (D, figure 4.7).
Tsebrenko found confirmation of this model by a series of experiments. One of the polymer blend systems under investigation was polyoxymethylene (POM) dispersed in a copolyamide (CPA). Using dismountable capillaries and by freezing the extrusion equipment at any state in liquid nitrogen, he found that the fiber-forming particles coalesce and stretch to form fibrils in the entrance zone.
At this point it should be stressed, that not all given polymer combinations will exhibit fibrillation as described above: There are a number of conditions that have to be fulfilled before perfect fiber formation takes place. These conditions have been examined by a number of research workers, and the results of these investigations will be presented below.

4.4.3 *Rheological parameters*

One of the first parameters that appears to play a predominant role in fibrillation during extrusion of a dispersion of a fiber forming polymer in another polymer is the viscosity ratio of the two phases η_1/η_2; η_1 = the viscosity of the matrix polymer and η_2 = the viscosity of the fiber-forming polymer. The value of η_2/η_1 should be about or equal to unity in order to obtain a more or less regular or perfect fiber structure as is shown by Vinogradov [53] and Tsebrenko [51,54]. If $\eta_2/\eta_1 < 1$ besides fibrillation also formation of films occur. This

remarkably also happens sometimes when $\eta_2/\eta_1 > 1$; when $\eta_2/\eta_1 > 10$ the extrudate mainly contains particles of the fiber forming component with the same dimensions of the original particles, indicating that no deformation has occurred. This observation is in agreement with the description of Cox [45], as can be seen from Elmendorp's work [43].
Tsebrenko also discovered that a high degree of fibrillation is coupled with a high die swell of the extrudate; the highest swelling was detected in the case where η_2/η_1 had a value close to unity. Unfortunately, this die-swell leads to a partial destruction of the uniaxial alignment of the fibers; this problem can be overcome by drawing down the extruded thread, and in some cases an even higher degree of fiber orientation and a more uniform fiber diameter distribution can be achieved [55].
Most results were obtained by selective dissolution of the matrix component from the extrudate and examining the bundles of fibers by microscopy.
The second parameter that appears to play an important role is the wall shear stress, taken as a macroscopic measure for the stress conditions under which the blend is extruded into and through the capillary.
It appears that there is an optimum in the shear stress where the largest number of fibers are being formed, and where the extrudate contains no other kinds of structures like films and/or powders.
If the shear stress is smaller or larger than the optimum value, the average fiber diameter increases, the number of fibers decreases and short irregular fibers, as well as films and powders can be formed. If the shear stress is very large the regular microstructure of the extrudate is even totally destroyed.
The viscosity ratio and the shear stress conditions can be combined to give a general picture of the mutual dependence of these parameters as is shown in figure 4.8.
In figure 4.8 the region where perfect fiber formation takes place has two sharp boundaries; The sloping line (separating regions B and C) was empirically found to obey the following relation:

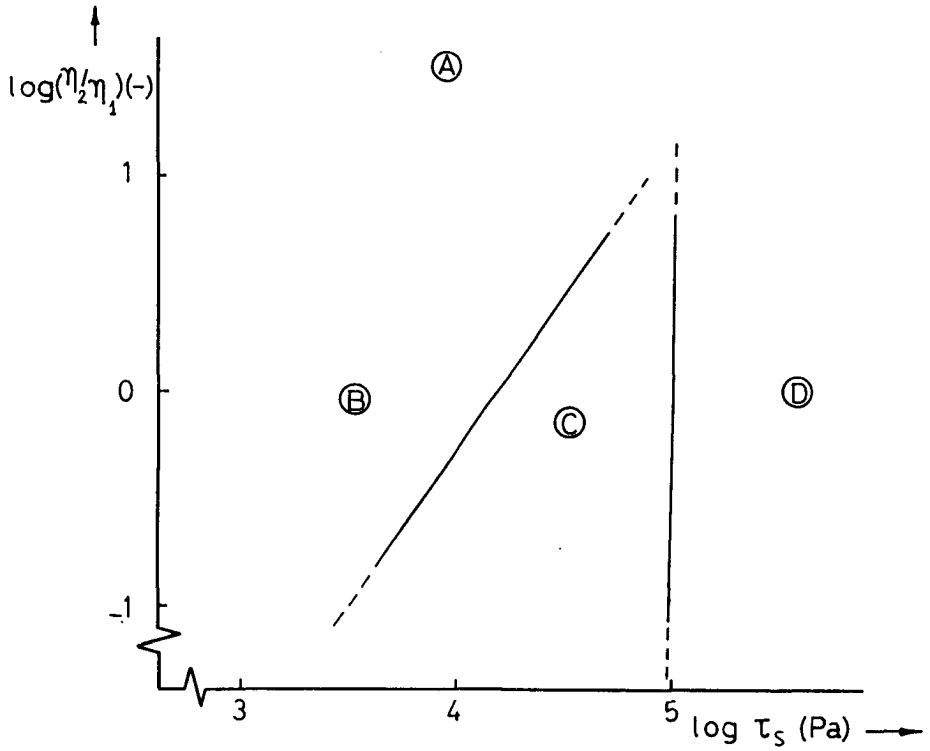


Fig.4.8 Viscosity ratio η_2/η_1 versus shear stress τ; A. no fibers, B. imperfect fibers, C. perfect fibers, D. disintegrated fibers.

$$\tau_{cr} = 1.6 \cdot 10^4 \ (\eta_2/\eta_1)^{0.7} \ \text{(Pa)} \qquad (25)$$

where τ_{cr} = the critical shear stress
η_1 = the viscosity of the matrix component, and
η_2 = the viscosity of the fiber-forming component of the blend.

(The factor $8 \cdot 10^4$ instead of $1.6 \cdot 10^4$, as mentioned by Vinogradov [53], is in disagreement with his graph of η_2/η_1 versus τ, and is probably caused by a reading error).
The other line (separating regions C and D) represents the limiting value of the shear stress (τ_{lim}) which is (at least according to Vinogradov) hardly influenced by the viscosity ratio of the mixture.
The lower boundery of the region of perfect fiber formation is not accurately known, but a viscosity ratio that is too low causes the

fibers to desintegrate into droplets during flow through the capillary. Also films are formed in that case. Anyway, there appears to be a distinct region of shear stresses in relation to the viscosity ratio where perfect fibers can be formed during extrusion of an incompatible polymer blend through a contraction and a capillary.
The influence of the shear stress can also be shown by varying the capillary dimensions (represented by the ratio of the capillary length and diameter L_c/D_c). Results from different research workers [56,57] show that there is always a tremendous influence of the capillary dimensions on the type of structure in extrudates of polymer mixtures, and in many cases an optimum in the L_c/D_c-ratio is found at which a perfect fibrillar morphology with uniaxial alignment is formed.

D_c, µm	Continuous length fibers				Short fibers			Particles			Films	
	d, µm	total number	% by weight	% by number	d, µm	% by weight	% by number	d, µm	% by weight	% by number	% by weight	% by number
396	4.5	2160	81.9	60.1	4.3	17.6	30.0	4.0	0.5	10.0	0	0
495	5.1	3430	90.3	69.7	4.3	9.7	28.4	5.6	0	1.9	0	0
594	5.5	3950	93.4	80.3	4.7	6.6	19.4	3.6	0	0.3	0	0
780	5.5	6800	100.0	100.0	-	0	0	-	0	0	0	0
820	5.9	9330	100.0	100.0	-	0	0	-	0	0	0	0
1250	6.4	16000	88.4	88.4	3.8	2.0	11.1	3.6	0	0.2	4.6	0.3
2130	8.1	18400	69.8	69.8	6.7	8.5	28.7	4.0	0	1.0	10.4	0.5

Table 4.9 Effect of capillary diameter on types of structure in extrudates of POM-CEVAc mixtures; L_c = 16 mm.

Naturally the ratio of the diameters of the reservoir and the capillary plays an important role; this ratio must be large enough to achieve a sufficient degree of stretching.
For mixtures of polyoxymethylene (POM) and ethylene-vinyl acetate copolymer (CEVAc) an optimum in the L_c/D_c-ratio of 20 is reported (see table 4.9).
Another factor influencing morphology development in a two-phase polymer flow is the temperature. Of course it must be higher than the softening point of both materials involved in order to achieve any deformation of the dispersed phase at all, at least under normal conditions. Furthermore the degree of fiber dispersion is reported to increase with increasing temperature [50,56] combined with formation of more uniform fibers. Ablasova [56] explained this observation by a decreasing blend melt viscosity with rising temperature causing

earlier coalescence of the dispersed particles.
The fiber formation is also influenced by the particle size of the dispersed phase in the starting material. For blends of polyoxymethylene (POM) and a copolyamide (CPA) an optimum particle size of 1.5 μm is reported [51]; above this size the fibers are less uniform and the blends show a less regular morphology; starting from a particle size smaller than 1.1 μm the extrudate contains large amounts of powder and/or very short fibers. This phenomenon can be explained by the fact that below this critical particle size, at least for this polymer combination and under these specific circumstances, the interfacial forces will dominate the deformational forces [58] causing break-up of the fibers by capillary instabilities [43].

4.5 *Experimental investigation of fiber formation conditions*

4.5.1 *Equipment and method*

For the fiber formation experiments a capillary rheometer with a barrel diameter of 20 mm was used. We were able to prepare bars of the polymer mixture that exactly fit in the rheometer's barrel on forehand; these bars were manufactured by mechanically mixing the two phases, either granules, screen fractions of ground granules, or powders, and heating the mixture under vacuum in a special mould followed by cooling under pressure (15 MPa). The heating time and temperature were chosen in such a way that a mechanically coherent bar was obtained; complete melting of both materials was not required and unnecessary degradation as well as distortion of the particle distribution by density gradients could be avoided.
These pre-manufactured bars were inserted in the rheometer barrel which had already been adjusted to the desired temperature. The polymer mixture was conditioned for a period of 30 minutes to obtain a uniform temperature throughout the whole barrel.
The rheometer could be mounted with three capillaries, all with a conical entrance (90°), a diameter of 1.634 mm, and with respective lengths of 15.0 mm, 30.0 mm and 75.0 mm. The piston speed could be varied stepwise resulting in apparent shear rates ranging from 0.3934

s^{-1} to 1967 s^{-1}. Just above the conical entrance a pressure transducer was mounted.
From the samples of the various polymer mixtures (for materials: see section 4.5.2) that were extruded under different conditions, the matrix material was extracted with a selective solvent in a Soxhlet extraction device. The resulting fraction was examined with a light microscope to elucidate its microstructure.

4.5.2 *Materials*

The following polymer combinations were chosen to examine the fiber forming behaviour as a function of the rheological parameters:

1) 30 weight % HDPE, Stamylan 8760; MFI = 0.06 dg/min (2 kg at 190°C)
   70 weight % PS, Hostyren N2000; MFI = 26 dg/min (5 kg at 200°C)
2) 30 weight % HDPE, Stamylan 8760
   70 weight % PS, Hostyren N4000; MFI = 4.5 dg/min (5 kg at 200°C)

Prior to the experiments with the polymer blends viscosity measurements of all individual polymers were performed with the aid of the same capillary rheometer. On treating the results from the blend experiments as a first approximation the viscosity values at the corresponding wall shear stress were used to calculate the viscosity ratio in the blend. The pressures measured during the blend extrusion were used to calculate the corresponding shear stresses. Experiments were performed at three temperatures: 160°C, 170°C and 180°C.

4.5.3 *Results*

The polymer combinations will be treated in successive order; the observed microstructure of the extruded blend is presented in a fashion corresponding to figure 4.9.
In figure 4.10 the results of combination 1 (see section 4.5.2) are summarized.
One can clearly see that a number of experiments yielded perfect fibers throughout the bulk of the extruded blend. Surprisingly, this

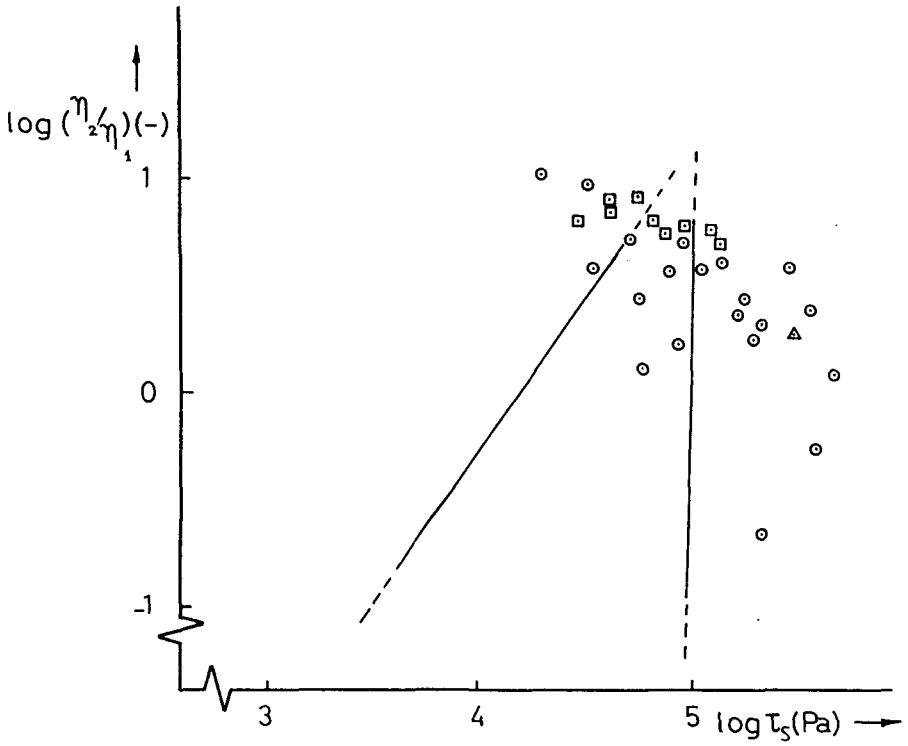


Fig.4.10 Fiber formation as a function of shear stress and viscosity ratio for combination 1 (see text) at different temperatures. ⊡ = perfect fibers, ⊙ = fibers in concentric shells, Δ = powders and/or disintegrated fibers.

does not happen at a viscosity ratio of 1; the most probable explanation is that during extrusion the viscosities as plotted in figure 4.10 of both phases are not exactly known, but are taken from capillary rheometer measurements of the bulk material at corresponding shear stresses (see section 4.5.2). Consequently the viscosity ratio in the flowing polymer blend might be lower than appears from figure 4.10. Unfortunately not enough information is available to estimate the corrected viscosity values.

From these experiments it can also be concluded that the region of perfect fiber formation is not as sharply restricted as is suggested by Vinogradov [53]; also in the regions B (Vinogradov: imperfect fibers) and D (Vinogradov: disintegrated fibers) perfect fiber

formation was detected in several cases.
The most plausible explanation for this discrepancy might be the influence of the entrance angle; Vinogradov's boundaries (see section 4.4.2) were based on experiments where the entrance angle was 180°, while the experiments presented here are all performed with an entrance angle of 90°. Indeed, in an earlier paper [59] Tsebrenko and coworkers recommend an entry angle of 120° for the practical purpose of producing ultrafine fibers from a melt of mixed polymers. Amazingly enough this recommendation is not taken into account in later publications where the entrance angle was chosen to be 180° [53].
As can be seen in figure 4.10, in many cases the extrudate consisted of a number of concentric shells which enclosed a strand of more or less perfect fibers (schematic drawings of this morphology and of perfect fibers only are shown in figure 4.11). This extrudate morphology was found even further away from the "perfect fiber"-region; this result might also be mainly due to the effect of the entrance angle.

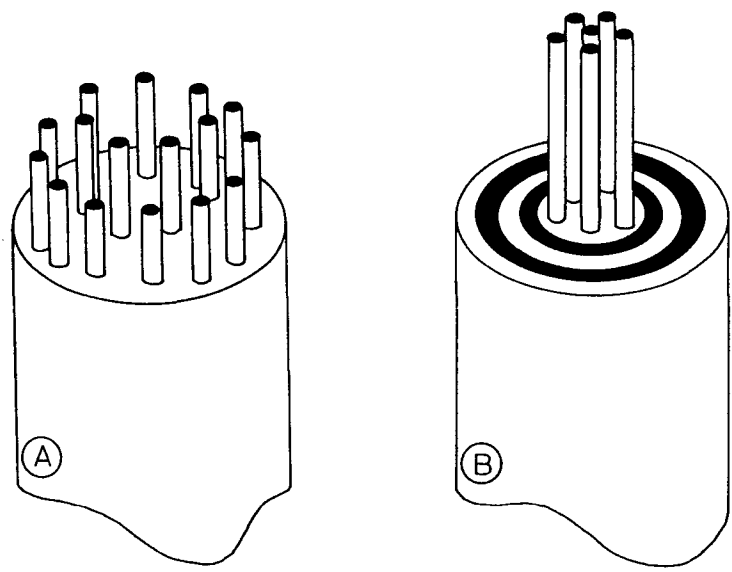


Fig.4.11 Schematic drawing of extrudate morphology; a: perfect fibers, b: fibers in concentric shells.

The results of combination 2 (section 4.5.2) are summarized in figure 4.12. Unexpectedly perfect fibers were never found during these experiments; a possible explanation is that the viscosity ratio after corrections as suggested above is smaller than unity; indeed, the extrudates were always found to have an outer shell of HDPE indicating that this material probably had the lowest viscosity during extrusion. With this material combination a larger number of samples contained desintegrated fibers and/or powders; in all those cases severe melt fracture of the extrudate was detected, suggesting a strong relationship between these two phenomena.

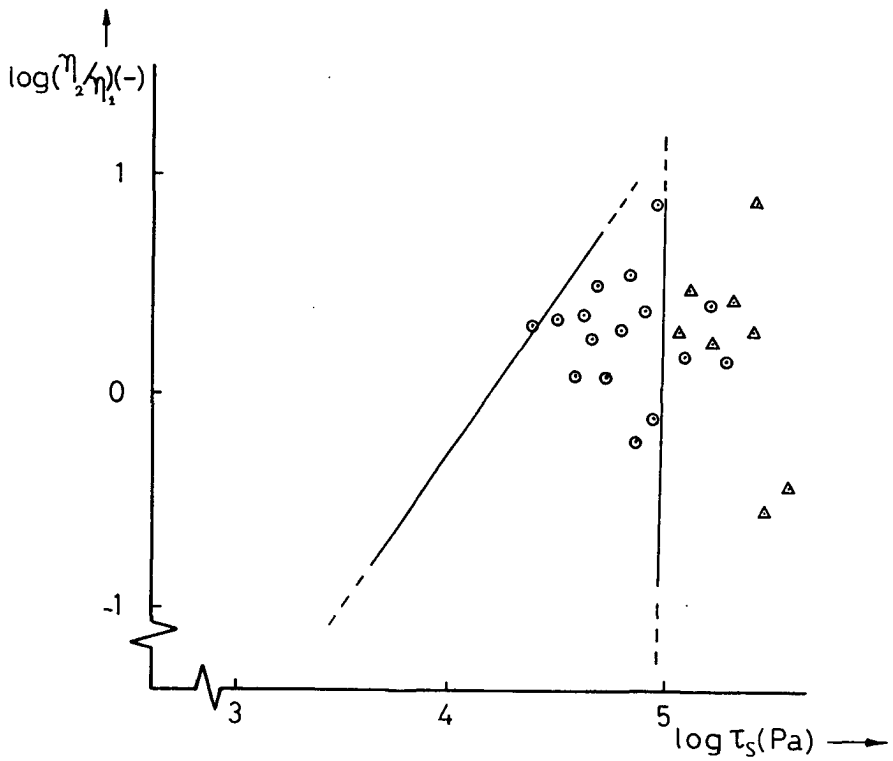


Fig.4.12 Fiber formation as a function of shear stress and viscosity ratio for combination 2 (see text) at different temperatures. ⊙ = fibers in concentric shells, Δ = powders and/or disintegrated fibers.

5 The relaxation behaviour of a stretched polymer melt

5.1 *Introduction*

As already mentioned in section 3.3, the relaxation behaviour of a stretched polymer melt after elongational flow plays a very important role in establishing the delicate balance between deformation, relaxation and crystallization. This relaxation behaviour is not easy to determine experimentally; we are dealing with a molten polymer with which very precisely defined experiments have to be performed accurately in order to measure stress development during and stress relaxation after purely uniaxial elongational flow. Forces as low as 10^{-3}N have to be determined with a reasonable accuracy and reliability. Moreover, preparation of the samples has to be performed with very great care.
In this chapter two different theoretical descriptions of the relaxation behaviour of polymer melts after elongational flow will be given and they will be compared with a series of experimental data, as measured at the Koninklijke/Shell Laboratories in Amsterdam, where a Rheometrics Extensional Rheometer (RER 9000) was available and kindly put to our disposal.

5.2 *Theoretical models*

There have been numerous efforts to describe the stress response of molten polymers in almost any kind of flow, but in many cases the validity of the proposed models is subject to a number of more or less serious restrictions. For instance, linear response is only found to occur in the case of very small deformations at very low deformation rates. In any other case there is always a notable deviation between theory and experiment.
Although this last observation is not very motivating, the reason for this continuous quest for a decent description of the stress response is obviously the (almost) impossibility to measure this response for any material under any circumstance with the aid of a fast and easy method. Indeed, the opposite is usually true and a satisfactory

theoretical model would overcome a lot of experimental trouble.
In the framework of this project until now only two existing models have been taken into consideration, namely the constitutive equations as proposed by Lodge and as proposed by Wagner. These two will be treated here in succesive order.

5.2.1 *Lodge's constitutive equation*

Already in 1956 Lodge introduced a linear model for the stress response of polymeric liquids in well-defined flow fields [60]. The constitutive equation reads as follows:

$$p_{ij}(t) = -p_0\,\delta_{ij} + \int_{-\infty}^{t} \mu(t-t')\,c_{ij}^{-1}(t,t')\,dt' \qquad (26)$$

where $p_{ij}(t)$ = the i,j-component of the stress tensor;
δ_{ij} = the Kronecker delta;
p_0 = the isotropic stress contribution;
$c_{ij}^{-1}(t,t')$ = the i,j-component of the relative Finger strain tensor;
$\mu(t-t')$ = the memory function;
t = actual time;
t' = time of deformation ($t' \leq t$)

Since we are particularly interested in the stress relaxation behaviour, we have to calculate the stress decay after uniaxial elongational flow with a constant extensional rate q_e during a period from t_0 to t_1. In this case the components of the Finger tensor are given by

$$c_{11}^{-1}(t,t') = \exp\{2\epsilon(t,t')\};$$
$$c_{22}^{-1}(t,t') = c_{33}^{-1}(t,t') = \exp\{-\epsilon(t,t')\};$$
$$c_{ij}^{-1}(t,t') = 0 \text{ for } i \neq j.$$

The time dependent function $\epsilon(t,t')$ is represented by

$$\epsilon(t,t') = 0 \qquad t' \leq t_0$$
$$\epsilon(t,t') = q_e(t'-t_0) \qquad t_0 \leq t' \leq t_1$$
$$\epsilon(t,t') = q_e(t_1-t_0) \qquad t' \geq t_1$$

Substitution of these values gives the following calculation result:

$$(p_{11}-p_{22})_{t\geq t_1} = q_e \int_{t-t_1}^{t-t_0} \overset{0}{G}(s)\ \{2e^{2q_e(t_1-t+s)} + e^{-q_e(t_1-t+s)}\}\ ds \qquad (27)$$

where $\overset{0}{G}(s)$ = the shear modulus, for which holds

$$\mu(t) = -\frac{d\overset{0}{G}(s)}{ds} \qquad (28)$$

For this shear modulus we can also write

$$\overset{0}{G}(t) = \int_{-\infty}^{\infty} H(\tau)e^{-t/\tau}\ d(\ln \tau) \qquad (29)$$

Substitution of equation (29) in equation (27) gives the following expression for the stress relaxation after elongational flow:

$$(p_{11}-p_{22})_{t\geq t_1} = q_e \int_{-\infty}^{\infty} H(\tau)\cdot\tau\cdot e^{-(t-t_1)/\tau}\ \{\frac{2}{1-2q_e\tau}\cdot[1-e^{-(1-2q_e\tau)(t_1-t_0)/\tau}]$$
$$+ \frac{1}{1+q_e t}\cdot[1-e^{-(1+q_e\tau)(t_1-t_0)/\tau}]\}\cdot d(\ln \tau) \qquad (30)$$

where τ = relaxation time;
$H(\tau)$ = the relaxation time spectrum.

With the aid of this relatively simple equation the stress relaxation after elongational flow can be calculated without having to know the stress build-up during that elongational flow itself. It does take into account the finite period of time during which the elongation

took place; no stepwise deformation is assumed as has often been done in earlier considerations [61].
The logarithmic relaxation time spectrum can be determined from measurements of the storage and loss moduli of the material at small oscillatory deformation amplitudes.

5.2.2 *Wagner's constitutive equation*

Unlike Lodge's model, Wagner's semi-emperical constitutive equation [62-64] takes the dependence of the memory function upon the total strain into account by introducing a correction factor:

$$p_{ij} = -p_0 \cdot \delta_{ij} + \int_{-\infty}^{t} \mu(t-t') \cdot h(I_1, I_2) \cdot c_{ij}^{-1}(t,t')\, dt' \qquad (31)$$

where $h(I_1, I_2)$ is a damping function.

According to Wagner et.al. [65] this damping function is dependent on the first and second invariants of the Finger tensor, and it can be described as

$$h(I_1, I_2) = f \cdot \exp[-n_1\sqrt{(I-3)}] + (1-f) \cdot \exp[-n_2\sqrt{(I-3)}] \qquad (32)$$

where $I = \alpha \cdot I_1 + (1-\alpha) \cdot I_2$ (33)

I_1 = the first invariant of the Finger tensor

I_2 = the second invariant of the Finger tensor

In the case of uniaxial elongation the invariants are defined as

$$I_1 = \exp(2\epsilon) + 2\exp(-\epsilon) \qquad (34)$$

and $$I_2 = \exp(-2\epsilon) + 2\exp(\epsilon) \qquad (35)$$

where ϵ = the total Hencky strain = $\ln \frac{l}{l_0}$.

The parameters f, n_1, n_2 and α can be matched on the experiments and can subsequently be used to predict the material's response under different conditions.

In our case, again assuming uniaxial elongational flow starting at time t_0 and stopping at time t_1, the following equation for the subsequent stress relaxation is found:

$$(p_{11}-p_{22})_{t\geq t_1} = \int_{t-t_1}^{t-t_0} \overset{o}{G}(s)\, \frac{d}{d\sigma}\, [h(\sigma)\cdot(e^{2q_e\sigma} - e^{-q_e\sigma})]\, ds \qquad (36)$$

where $s = t-t'$

$\overset{o}{\sigma} = s-(t-t_1)$

$\overset{o}{G}(s)$ = the shear modulus.

In this case, unlike in the case of Lodge's constitutive equation, we do need the results of the stress build-up experiments during the elongational flow itself to calculate the damping function $h(t)$.

For this calculation the following equation is used:

$$\frac{d(p_{11}-p_{22})}{dt} = \overset{o}{G}(t)\, \frac{d}{dt}\, [h(t)\cdot(e^{2q_e t} - e^{-q_e t})] \qquad (37)$$

or

$$h(t) = \frac{1}{e^{2q_e t} - e^{-q_e t}} \int_0^t \frac{d(p_{11}-p_{22})/ds}{\overset{o}{G}(s)}\, ds \qquad (38)$$

Using equations (36) and (38), if the stress build-up in elongational flow with a constant extensional rate q_e is measured and if the shear modulus is known, the stress relaxation as a result of this deformation can be calculated.

5.3 *Experiments*

A series of experiments was performed with the aid of the Rheometrics Extensional Rheometer (RER 9000), which appears to be able to deal with the difficulties as described in section 5.1.
Cylindrical samples with a diameter of approximately 6 mm have to be prepared in a special mould: first of all the polymer granules are molten under vacuum to avoid degradation and air inclusion. When completely molten the material is forced into the mould, which consists of 15 parallel cylindrical holes. After filling, the mould is kept under pressure at a temperature above the melting point of the polymer for a certain period of time after which the mould is allowed to cool down slowly to room temperature, also still under pressure. After complete cooling the samples can be taken out and mechanically adapted to the desired length.
Next, these samples have to be glued to aluminium T-clips in order to be able to apply the elongational forces, without having to clamp the samples themselves in one way or another. To obtain a sufficient adhesion the samples must sometimes be etched with chromic acid and the T-clips sometimes need mechanical roughening. Epoxy is mostly used as the glueing material. Figure 5.1 shows a drawing of a ready-to-handle sample.

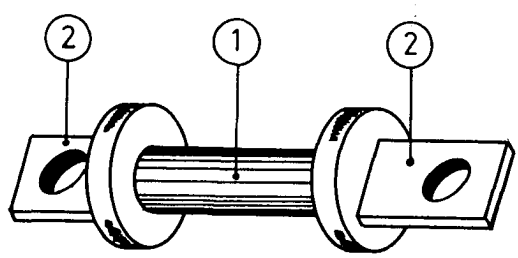


Fig.5.1 Sample, as prepared for measuring in elongational flow:
1. Cylindrical polymer sample, 2. Aluminium T-clip.

Samples of polyvinylidene fluoride (PVDF, Solef 1010) and of high-density polyethylene (HDPE, Stamylan 7031) were prepared by the method as described above with the following parameters:

For PVDF: Melting temperature 200°C
Pressure 10 MPa
Mould conditioning time 5 minutes
Cooling time approx. 120 minutes

For HDPE: Melting temperature 160°C
Pressure 10 MPa
Mould conditioning time 5 minutes
Cooling time approx. 90 minutes

Soon it became clear that measurements with HDPE would cause a number of very serious problems: to begin with, even after etching of the cylindrical polymer samples with chromic acid and mechanical roughening of the aluminium T-clips the adhesion after glueing was rather poor. The greater part of the assemblies broke apart during or shortly after mounting them in the measuring equipment. Those samples which survived handling could only be stretched at very low strain rates to low values of end deformation without exhibiting severe instabilities, constrictions and ultimately fracture of the sample, as could be easily observed both visually and by monitoring the shape of the stress build-up curve during the stretching experiment.
Preparation of the PVDF-samples appeared to be a lot easier; no etching of the polymer cylinders was required, and just a little roughening of the aluminium T-clips with abrasive coated paper was sufficient to achieve a good adhesion after glueing. The main restriction in this case was that the applied thermosetting adhesive (Uhu-Plus) seemed to degrade very fast at temperatures above 180°C, again causing disruption of the adhesive polymer-aluminium joint. Since the melting point of PVDF is also in that temperature region, no broad range of testing temperatures could be run through while using the same epoxy resin.
As a result of the considerations as given above only experiments with PVDF were performed. A series of samples was prepared following the procedure as described before, and they were elongated at 180°C with different strain rates to different end deformations. An overview of the flow parameters that were used, and where no instabilities like in

the case of the HDPE-samples were observed by any means, is given in table 5.2.

max. Hencky strain	Elongational rate (s^{-1})						
	0.005	0.05	0.1	0.25	0.5	1.0	6.0
1.0	+				+	+	+
2.5		+	+	+	+		

Table 5.2 Elongational flow parameters of measurements on PVDF at 180°C. ϵ_{max} *(maximum Hencky strain)* $= ln\ (l_{end}/l_o)$.

During flow the tensile stress build-up was recorded as a function of time.
After the flow was stopped the developed tensile stress was allowed to relax for a period of time, the length of which was chosen in relation to the duration of the elongation experiment. The decreasing stress could be monitored as a function of time, so a discrete stress relaxation curve was obtained (the sampling frequency of the RER 9000 is 40 Hz, and consequently, depending on the time scale chosen, a more or less stepwise curve is found for both stress build-up and relaxation).

5.4 *Results*

5.4.1 *Stress build-up and relaxation*

The stress growth curves for some of the experiments, as presented in table 5.2, are shown in figure 5.3 where the reduced normal stress $(p_{11}-p_{22})/q_e$ is plotted against time t. These curves show a normal behaviour for a polymer melt: at low elongational rates (in this case 0.005 s^{-1}) the reduced normal stress steadily increases until a plateau is reached, the height of which gives the value for the elongational viscosity of the material. For PVDF, Solef 1010 at 180°C this results in $\eta_e = 2.60 \cdot 10^5$ Ns/m^2.
At higher values of q_e the curves bend upwards at $t \approx 1/q_e$.

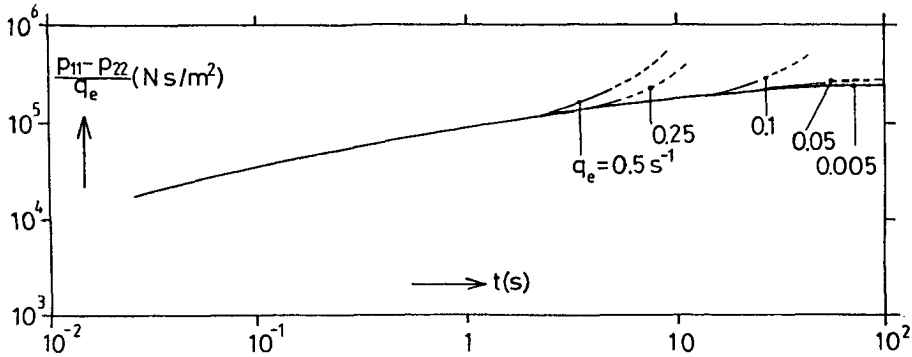


Fig.5.3 Growth of reduced stress, $(p_{11}-p_{22})/q_e$, of PVDF Solef 1010 at 180°C plotted against time for extensional flow to a maximum Hencky strain of 1 (——) and of 2.5 (---) at flow rates as indicated.

Figure 5.4 shows some experimental stress relaxation curves. One can clearly see that the relaxation is faster after elongation at higher flow rates. This is in qualitative agreement with Lodge's model when $\overset{0}{G}(t)$ is given as a sum of exponential terms:

$$\overset{0}{G}(t) = \sum g_i \exp(-t/\tau_i) \qquad (39)$$

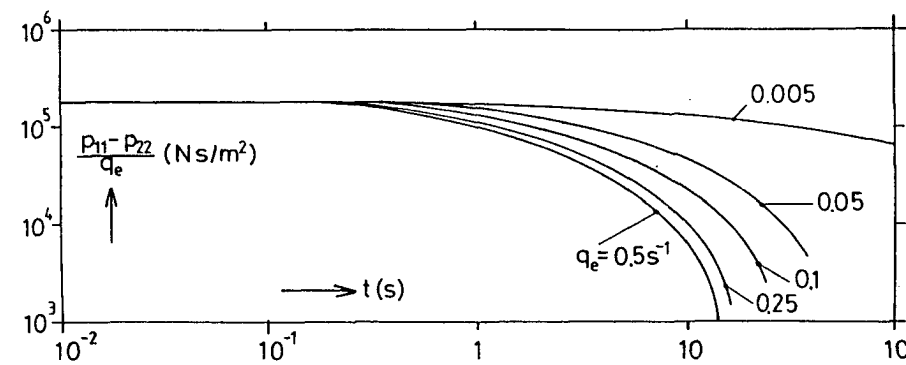


Fig.5.4 Relaxation of reduced stress, $(p_{11}-p_{22})/q_e$, of PVDF Solef 1010 at 180°C after extensional flow to a maximum Hencky strain of 2.5 at flow rates as indicated. In this case t is the time elapsed since cessation of the flow.

Also, Lodge's model predicts the sudden increase in normal stress; from equation (27) it follows that this phenomenon will take place under the condition $2q_e\tau_1 > 1$, where τ_1 = the longest relaxation time of the polymer under concern. While increasing the extensional rate q_e, more relaxation times will satisfy this condition resulting in an extra stress increase. On subsequent stress relaxation this extra stress will relax very fast, resulting in a faster over-all stress relaxation of the stretched polymer melt.

5.4.2 *The relaxation time spectrum*

To obtain the relaxation time spectrum of PVDF Solef 1010 at 180°C its storage and loss moduli were measured with the aid of a Rheometrics Mechanical Spectrometer (RMS 7200) at 180, 200 and 220°C (measurements kindly performed by Dr. Paul Leblans at DSM Research, Geleen, The Netherlands) and with a dynamic viscosimeter, mounted with an adapted measuring cell for polymer melts [66]. These data were reduced to 180°C using frequency-temperature superposition. The resulting mastercurves are shown in figure 5.5.

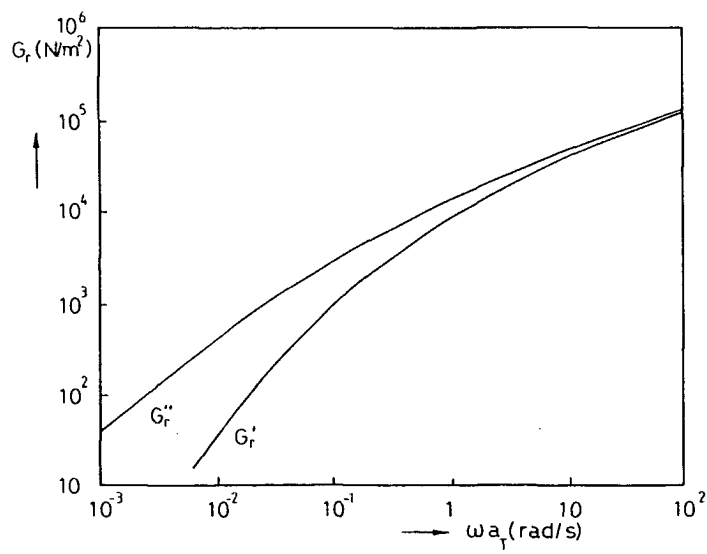


Fig.5.5 Mastercurves of storage and loss moduli of PVDF Solef 1010 at 180°C, plotted against the reduced angular frequency.

Using the approximation method as discussed by Scholtens and Booij [67], and as also described by Leblans [61], the relaxation time spectrum was calculated from the obtained mastercurve (calculations kindly performed by Dr. H.C. Booij and Mr. J. Palmen at DSM Research, Geleen, The Netherlands). This method is based on an approximative relation between the relaxation time spectrum and the loss modulus G" [68], which provides a first estimate of the distribution of the relaxation times in the time scale between $\tau_{min} = \omega_{max}^{-1}$ and $\tau_{max} = \omega_{min}^{-1}$, where ω_{min} and ω_{max} represent the lower and upper limits of the reduced frequency interval (figure 5.5). A number of succesive extrapolations and adjustments by comparing measured values of the loss angle ($\tan \delta = G''/G'$) with those calculated from the extrapolated relaxation time spectrum, ultimately yields this spectrum over a larger time scale [61].
The resulting relaxation time spectrum is shown in figure 5.6.

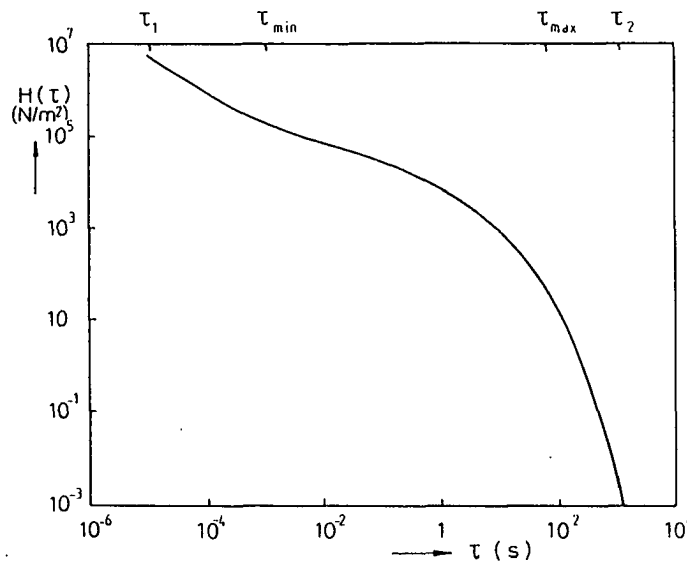


Fig.5.6 The relaxation time spectrum of PVDF Solef 1010 at 180°C.

From the relaxation time spectrum the shear modulus $\overset{0}{G}(t)$ can be calculated using equation (29). The result of this calculation is shown in figure 5.7.

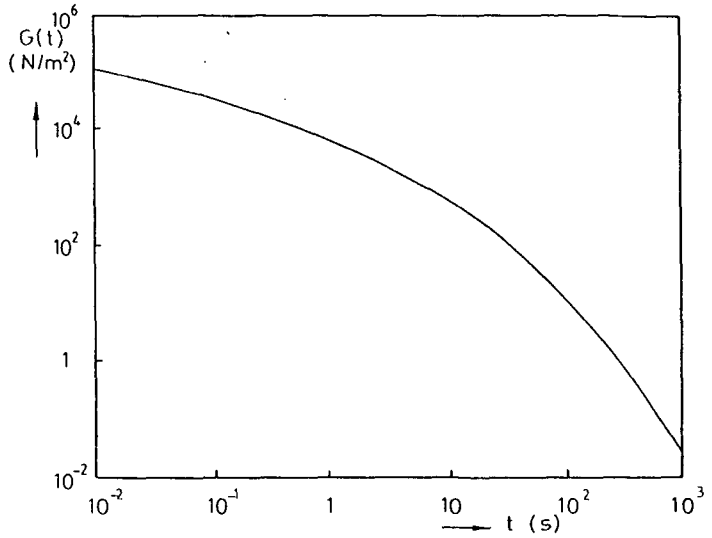


Fig.5.7 The shear modulus of PVDF Solef 1010 at 180°C as calculated from figure 5.6 using equation (29).

5.4.3 *Comparison with Lodge's constitutive equation*

Starting from the constitutive equation as proposed by Lodge [60] and knowing the relaxation time spectrum $H(\tau)$, the stress relaxation of a polymer melt after elongational flow with a constant extensional rate q_e during a period from t_0 to t_1 can be calculated from equation (30). Results of the calculations, using the same parameters as used in the experiments (table 5.2), taking $t_0=0$ and $t_1=\epsilon_{max}/q_e$, are presented in figure 5.8 together with the experimental results.

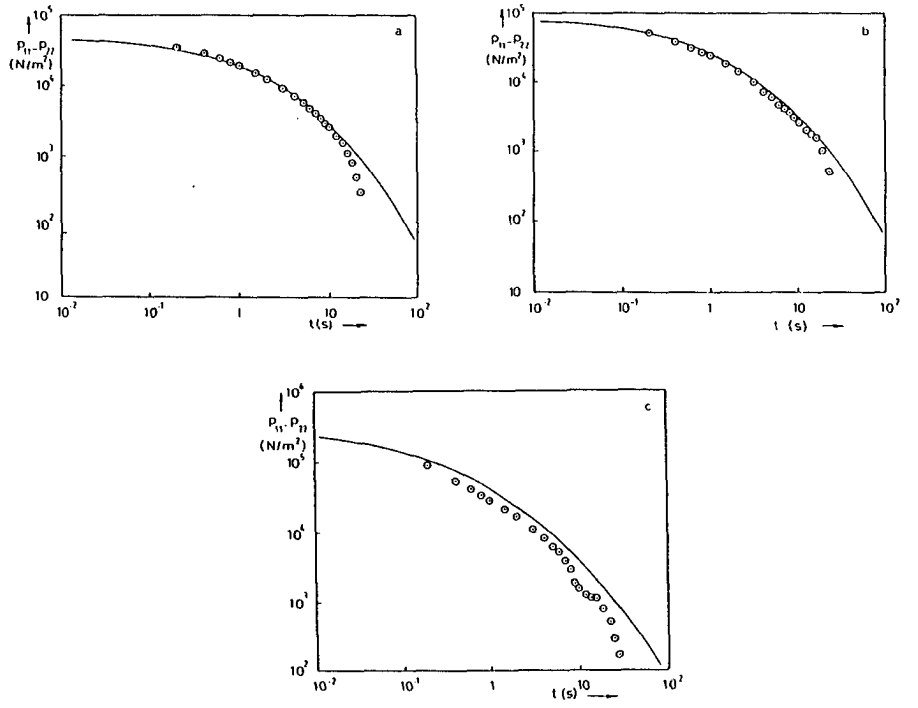
5.4.4 *Discussion*

From figure 5.8 (a through g) it follows that Lodge's constitutive equation predicts the relaxation behaviour of a polymer melt after elongational flow (as given by equation (30)) only in the case of relatively small maximum Hencky strains ϵ_{max}, and then again only for a relatively short period of relaxation (approximately 10 seconds at most). In the case of a higher ϵ_{max} there is already a deviation in

the starting level of the decaying stress, and the discrepancy only becomes larger on increasing the relaxation period.

The poor agreement between the experimental results and the theoretical predictions based on Lodge's constitutive equation can be mainly attributed to the nature of the memory function in equation (26); though it should actually be dependent on time, deformation and deformation rate, in this form it has no such dependency whatsoever. This qualitatively explains the reasonable agreement at low deformations, deformation rates and at a short time scale, and the large deviations in all other cases.

For maximum Hencky strains of 2.5 the experimental and theoretical starting stress levels can be matched by dividing the theoretical values by the value of the maximum Hencky strain [69]; there is no fundamental explanation for this fortuity, but it illustrates the necessity of a deformation dependent memory function.



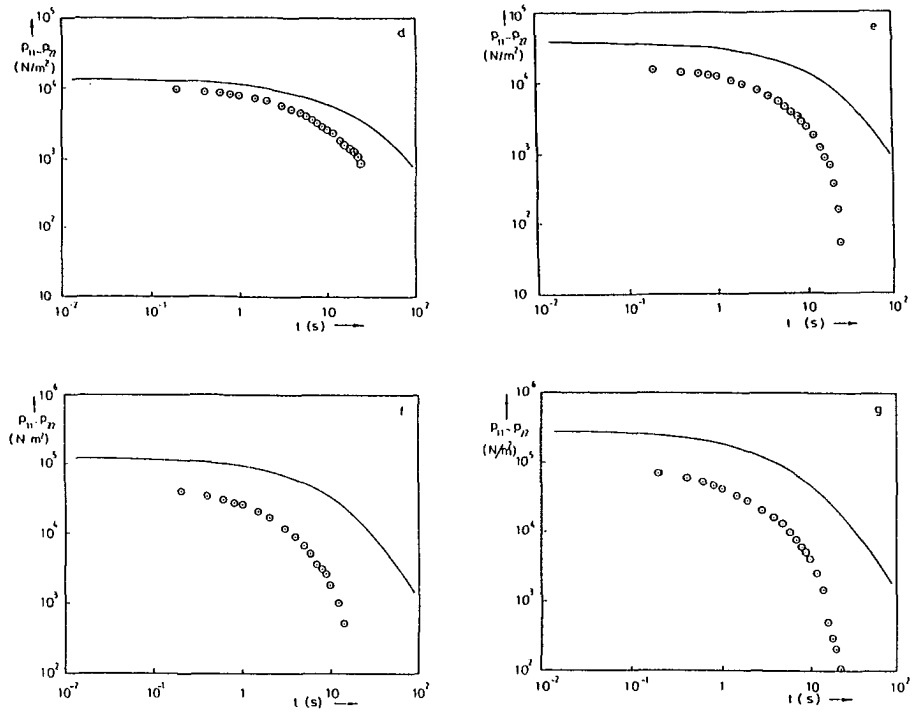


Fig.5.8 Stress decay of PVDF Solef 1010 at 180°C after elongation to a Hencky strain ϵ_{max}=1 (a through c) and to ϵ_{max}=2.5 (d through g) at various extensional flow rates: a) q_e= 0.5 s^{-1}, b) q_e= 1 s^{-1}, c) q_e= 6 s^{-1}, d) q_e= 0.05 s^{-1}, e) q_e= 0.1 s^{-1}, f) q_e= 0.25 s^{-1}, g) q_e= 0.5 s^{-1}.
⊙ experimental, (——) equation (30).

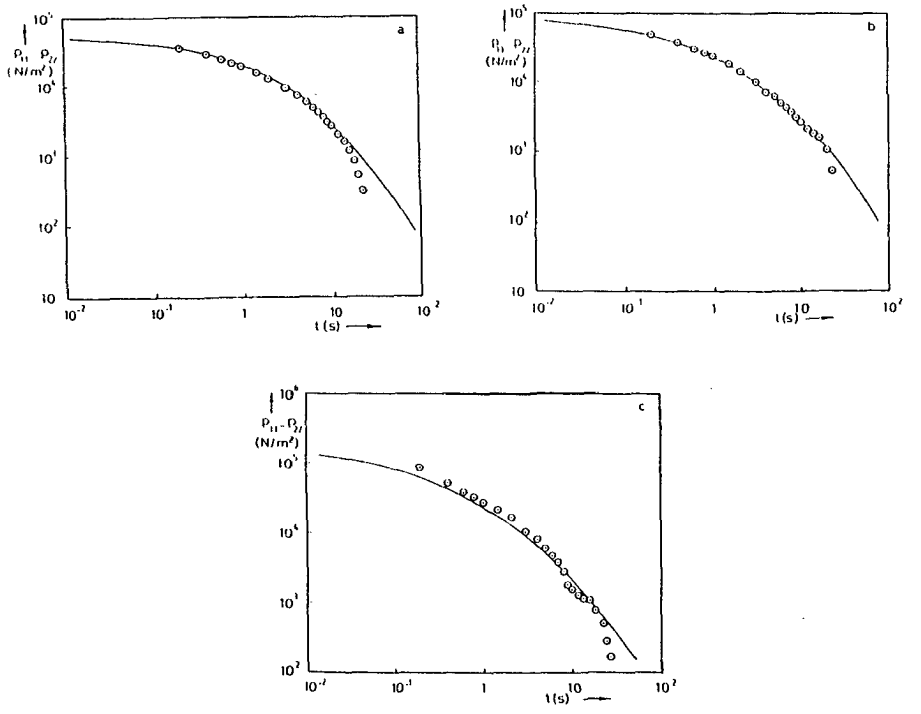
5.4.5 *Comparison with Wagner's constitutive equation*

The stress relaxation after elongational flow can also be calculated from Wagner's equations (36) and (38). Again, the results of the calculations, using the same parameters as used in the experiments (table 5.2) are shown in figure 5.9 together with the experimental results.

5.4.6 *Discussion*

The agreement between the experimental results and the theoretical predictions, based on Wagner's constitutive equation, is reasonably good; for both small and large end deformations ϵ_{max} the calculated starting level of the reduced stress $(p_{11}-p_{22})/q_e$ fits with the experimental data, and the experimental points follow the theoretical curve for an acceptable period of time for all values of the extensional flow rate q_e; in the case where $\epsilon_{max}= 1$ only after approximately 20 seconds the deviation between theory and experiment becomes inacceptably large.

In equation (31) the memory function $\mu(t-t',h)$ is factorized into a time dependent function $\mu(t-t')$ and a deformation dependent damping function $h(\epsilon)$. This assumption might not be allowed, but it is difficult to analyse the influence of this factorization on the



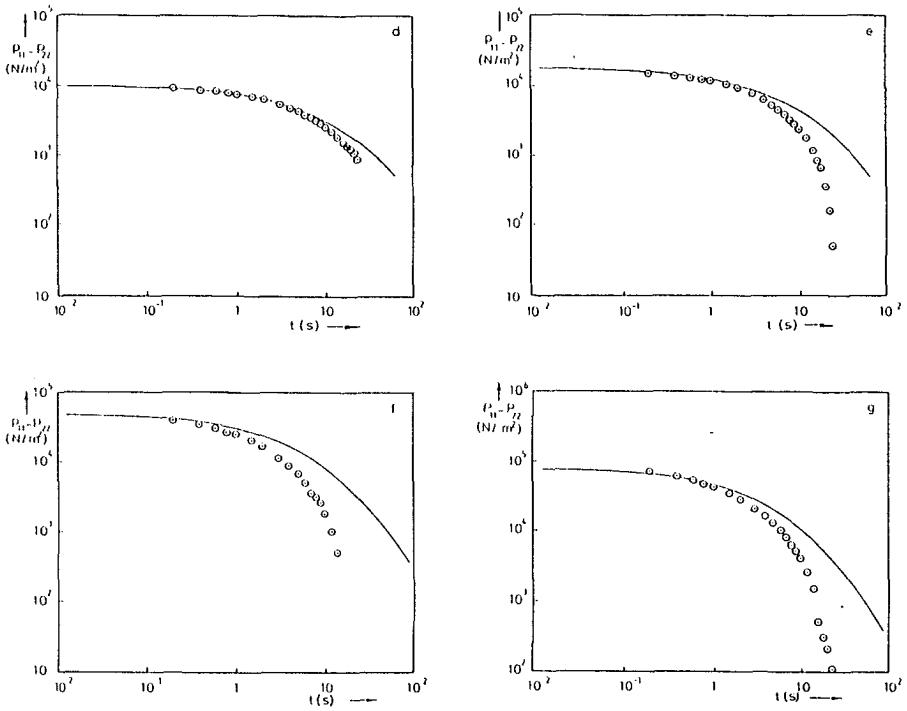


Fig.5.9 Stress decay of PVDF Solef 1010 at 180°C after elongation to a Hencky strain ϵ_{max}=1 (a through c) and to ϵ_{max}=2.5 (d through g) at various extensional flow rates: a) q_e= 0.5 s^{-1}, b) q_e= 1 s^{-1}, c) q_e= 6 s^{-1}, d) q_e= 0.05 s^{-1}, e) q_e= 0.1 s^{-1}, f) q_e= 0.25 s^{-1}, g) q_e= 0.5 s^{-1}.
⊙ experimental, (——) equation (36).

calculation results. A discussion of the dependence of the damping function on the extensional flow rate is given by Te Nijenhuis [70].

Although the experiments described in this chapter have been performed with PVDF only, it can be assumed that a good description of the relaxation behaviour of a stretched polymer melt with the aid of Wagner's constitutive equation is also possible for other polymers such as polyethylene and polypropylene. This provides a powerful tool for a more quantitative analysis of the balance between deformation and relaxation time scales, as mentioned in section 3.3, in future. Moreover, PVDF also shows the ability to form extended chain crystals by orientation-induced crystallization from the melt; in the scope of this work, a study of its relaxation behaviour after elongational flow can therefore be justified.

6 Scouting experiments

Based on the expectation that a crystallizable polymer, that would normally exhibit the anomalous behaviour as described in chapter 3 and ref. [31], would behave exactly the same when dispersed or embedded in another polymer, a series of experiments with two-phase polymer systems was performed where the only goal was to obtain fibers or threads that were formed by orientation-induced crystallization and hence consisted of extended-chain crystals.
These experiments were done in a number of different fashions: first of all we again have to distinguish between cocontinuous, concentric systems and dispersed systems. A second distinction is related to the nature of the experiment: either batch-wise (capillary rheometer) or continuous processing (extruders). Furthermore, a number of scouting experiments with the aid of a two-roll mill were performed. All tests are classified with regard to the distinctions as mentioned above.
In the case of extrusion, the extrudates were not drawn down, and they were allowed to solidify in contact with ambient air.

6.1 *Batch-wise coextrusion*

For these tests the same capillary rheometer as in the case of the fiber formation experiments (section 4.5.1) was used. This allowed for preparation of cocontinuous samples by first manufacturing a bar, 20 mm in diameter, of the matrix material (approximately following the method as also described in section 4.5.1), drilling a concentric hole of a fixed diameter along its axis, then manufacturing a small bar of the core material and assembling the two to create the test sample.

1) Matrix phase: PS, Hostyren N4000, MFI = 4.5 dg/min (5 kg at 200°C).
   Core phase: PP, Carlona P, type unknown, MFI = 15 dg/min (2.16 kg at 230°C).
   Initial core diameter: 5 mm.
   Temperature: 165°C (barrel), 155°C (capillary).
   Capillary: conical entrance (90°), D_c= 1.634 mm, L_c = 75.0 mm.
   Mechanical separation of the coextruded materials.

At an apparent shear rate of 50 s^{-1} a fairly regular polystyrene extrudate was formed, containing a continuous core of polypropylene. The fiber could be easily removed from the brittle matrix and appeared to be oriented in comparison with the same material as extruded at higher temperatures, both observed with the aid of a polarization light microscope and as shown in the WAXS pattern (figure 6.1). Due to irregularities in its shape as a result of mild flow instabilities its mechanical properties could not be established with certainty, but measurements showed that its Young's modulus was probably higher than 3 GPa and its tensile strength considerably higher than 200 MPa (values for an unoriented PP-sample are 1.3 GPa and 50 MPa, respectively).
These values can also be reached with the aid of a common fiber spinning process; therefore it may be assumed that the material consists of oriented folded-chain crystals.

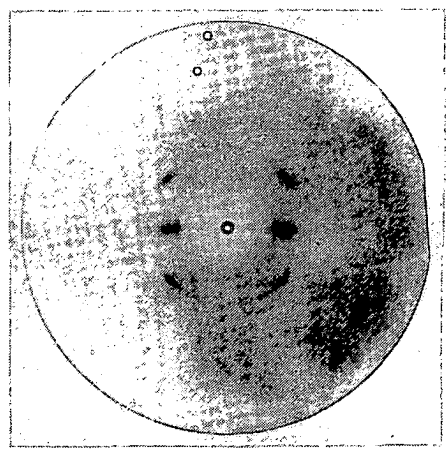


Fig.6.1 WAXS-pattern of oriented PP-fiber (see text for discussion).

2) Matrix phase: PS, Hostyren N2000, MFI = 26 dg/min (5 kg at 200°C).
Core phase: POM, Delrin 150 SA, MFI = 1 dg/min (2.16 kg at 200°C).
Initial core diameter: 3 mm.
Temperature: 177 - 180°C.
Capillary: conical entrance (90°), D_c = 1.634 mm, L_c = 75.0 mm.
Mechanical separation of the coextruded materials.

In the temperature region as mentioned above, a regular cocontinuous thread could be extruded at shear rates ranging from 20 s^{-1} to 200 s^{-1}. DSC-analysis of the POM-samples after peeling off the PS-shell showed melting points of 186 ± 2 °C; second scans of the same samples yielded the "normal" value of 177 ± 1 °C. However, WAXS-analysis of these samples showed no crystalline orientation at all. Again we have to conclude that no ECC-morphology was formed.

6.2 *Continuous coextrusion*

With the same coextrusion equipment as has been used for studying the deformational behaviour of concentric, cocontinuous two-phase systems (see section 4.3.1), different material combinations at many different conditions were tested for their ability to produce highly oriented threads of the embedded crystallizable core material.

1) Matrix phase: PS, Hostyren N2000, MFI = 26 dg/min (5 kg at 200°C).
   Core phase: PP, Carlona P S6100, MFI = 11 dg/min (2.16 kg at 230°C).
   Matrix mass flux: 18.0 g/min and decreasing.
   Core mass flux: 9.0 g/min.
   Temperature: die temperature settings decreasing from 190 to 170°C.
   Die: conical entrance (90°), capillary (D_c= 2 mm, L_c = 120 mm).
   Mechanical separation of the coextruded materials.

While decreasing the die temperature settings stepwise by 5°C every 30 minutes, the stability of the coextrusion process could only be maintained by decreasing the screw speed of the extruder supplying the matrix material (the other extruder, supplying the core material, was already operating at its lowest speed). The actual melt temperature was not measured.
In the temperature region 180-175°C a substantial and increasing die-swell was noted, indicating a high degree of elastic deformation.
Maintaining the coextrusion stability was only possible at matrix mass fluxes of 9.0 g/min and slightly lower.
In one occasion, shortly before severe instabilities and blocking of

the capillary by a plug of crystallized PP occurred, a thread containing a solid PP-core of 1.14 mm diameter and about 50 mm length was extruded [71]. After peeling off the PS-shell this sample was investigated by DSC- and WAXS-analysis.

The DSC-scan of the coextruded sample showed two peaks (figure 6.2): one small peak at 156 ± 2 °C and a large peak at 178 ± 2 °C. A second scan of the same sample after recrystallization in the DSC-unit yielded the "normal" melting peak for PP of 160 ± 2 °C (figure 6.3).

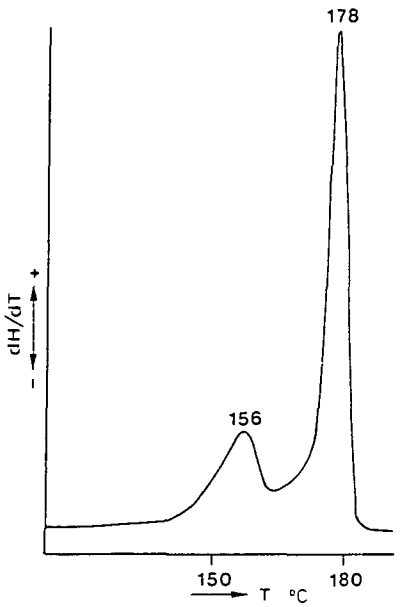


Fig.6.2 DSC-scan of a highly oriented thread of PP (Carlona P S6100) formed by coextrusion with PS (Hostyren N2000); scan speed 16°C/min. See text for discussion.

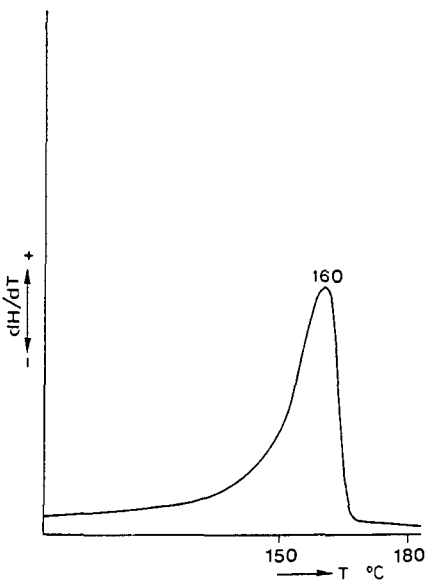


Fig.6.3 DSC-scan of the same sample as in figure 6.2 after recrystallization in the DSC-unit; scan speed 16°C/min. See text for discussion.

The WAXS-pattern of the sample shows the typical pattern for a highly oriented crystal morphology: sharp points (figure 6.4) instead of rings, as in the case of an unoriented folded-chain crystal morphology (figure 6.5). The faintly visible layer lines suggest a single crystal-like structure. Analysis of the diffraction pattern yields a monoclinic unit cell (see table 6.6).

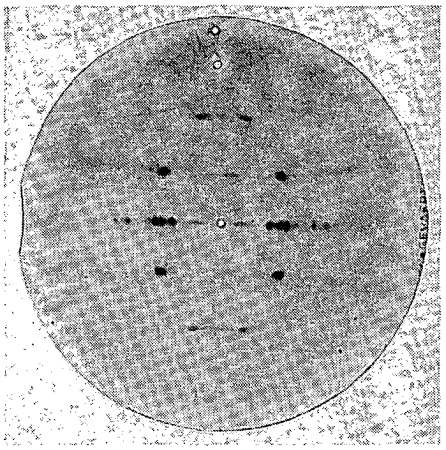


Fig.6.4 WAXS-pattern of highly oriented PP-thread.

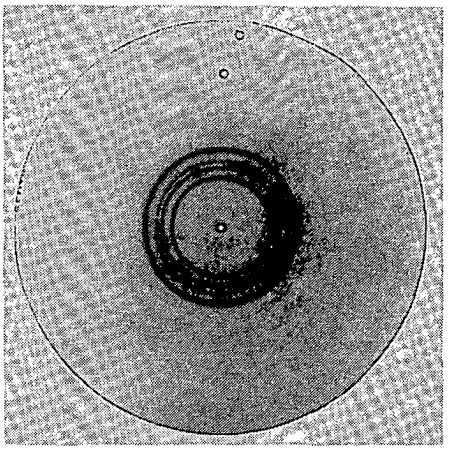


Fig.6.5 WAXS-pattern of unoriented PP-thread.

	2x	2y	c_{exp}	c_{mon}	d_{exp}	d_{mon}	H K L
0	23.8	-	-		6.35	6.26	1 1 0
	29.2	-	-		5.23	5.24	0 4 0
	31.8	-	-		4.83	4.78	1 3 0
	45.5	-	-		3.51	3.49	0 6 0
	51.3	-	-		3.16	3.13	2 2 0
1	28.0	24.3	6.52	6.50	4.20	4.07	1 2 1
	29.7	24.3	6.55	6.50	4.07	4.06	0 4 1
	6±1	23.2	6.57	6.50	6.31	6.13	0 1 1
2	12±0.5	51.5	6.55	6.50	3.09	3.07	0 2 2

Table 6.6 Analysis of WAXS-pattern of highly oriented PP-thread.
c_{exp}, d_{exp} = experimental c- and d-values;
c_{mon}, d_{mon} = monoclinic c- and d-values.
Experimental c- and d-values calculated following ref.[72].

Also the flexural modulus of the rod was determined by clamping it on one side and then bringing it into vibration. The vibrational frequency, clearly in the hearing range, was tape-recorded. Visualizing the play-back signal on an oscilloscope yielded a frequency of 514 Hz. Using

$$E = \frac{4\,\pi^2\,f^2\,\rho\,l^4}{3.09\,a^2} \qquad (40)$$

where E = flexural modulus (Pa)
f = vibrational frequency (Hz)
ρ = density (kg/m^3)
l = length of the rod (m)
a = radius of the rod (m),

the flexural modulus can be calculated. Taking f = 514 Hz, ρ = 910 kg/m^3, l = $35.25 \cdot 10^{-3}$ m and a = $0.57 \cdot 10^{-3}$ m, this results in a modulus of 14.6 GPa.
The theoretical maximum for the Young's modulus is 42 GPa, so it is clear that the high orientation, as already shown by the DSC- and WAXS-analysis, gives rise to a dramatic increase in stiffness.
In this case it can be concluded that a large fraction of the sample's crystalline phase is in the ECC-configuration.

2) Matrix phase: PS, Hostyren N2000, MFI = 26 dg/min (5 kg at 200°C).
Core phase: POM, Delrin 150 SA, MFI = 1 dg/min (2.16 kg at 190°C).
Matrix mass flux: 6.6 g/min.
Core mass flux: 17.4 g/min.
Temperature: varying from 160 to 190°C.
Die: conical entrance (120°), capillary (d = 3 mm, l = 30 mm).
Mechanical separation of the coextruded materials.

By varying the temperature settings of both extruders and the die sections a number of samples at different core melt temperatures (measured with a thermocouple, mounted perpendicular to the flow direction) were taken and tested for their mechanical properties; the mass fluxes of both components were not appreciably changed by varying

the temperature settings.
The results of the measurements of the Young's moduli are presented in figure 6.7 as a function of the measured core temperatures.

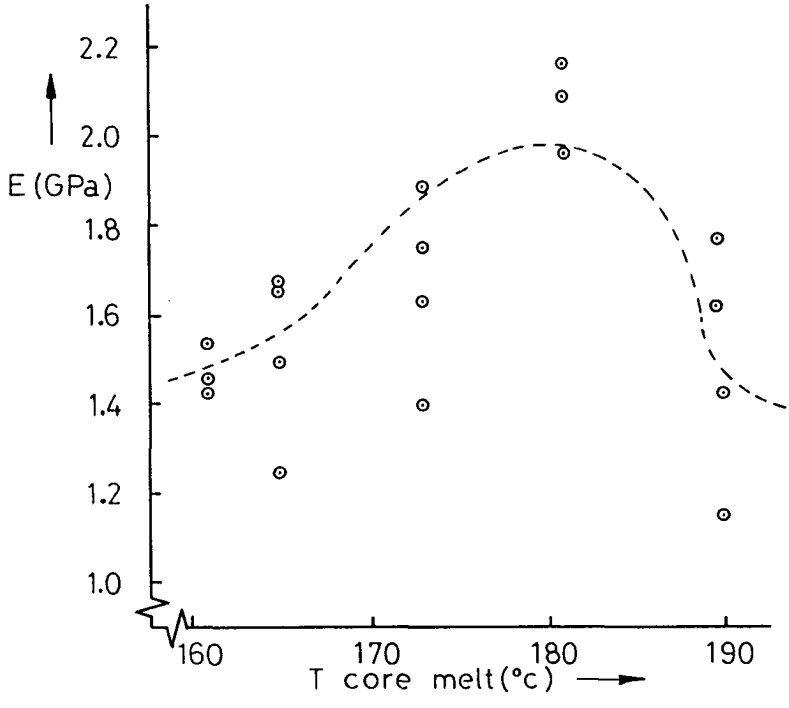


Fig.6.7 Young's moduli of POM, Delrin 150 SA, after coextrusion in a matrix of PS, Hostyren N2000, as a function of the measured core melt temperatures. See text for discussion.

One can clearly see that there is an optimum in the Young's modulus at a core melt temperature of about 180°C; however, the corresponding value of 2 GPa does not indicate the existence of an extended chain crystal (ECC) morphology. Indeed, the crystalline melting point as determined by DSC-analysis was found to be 179°C, which is only 2°C higher than the "normal" value; a substantially higher melting point might be expected if the sample were to contain ECC's.

3) Matrix phase: PS, Hostyren N3000, MFI = 11 dg/min (5 kg at 200°C).
Core phase: PP, Carlona P S6100, MFI = 11 dg/min (2.16 kg at 230°C).
Matrix mass flux: 18.6 g/min.
Core mass flux: 9.3 g/min.
Temperature: varying from 170 to 180°C.
Die: conical entrance (120°), capillary (D_c = 3 mm, L_c = 30 mm), sometimes glass windows.
Mechanical separation of the coextruded materials.

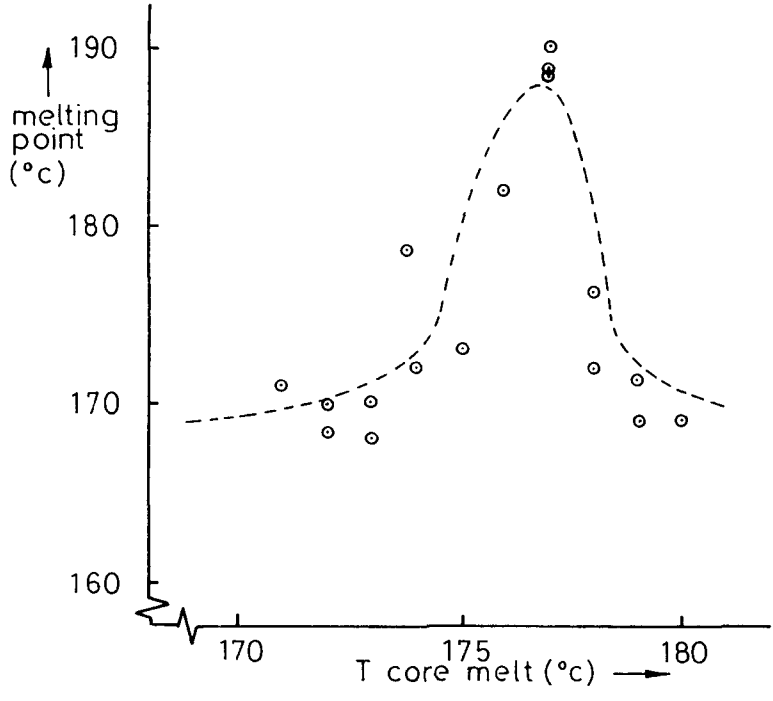


Fig.6.8 Melting points as determined by DSC-analysis of polypropylene, Carlona P S6100, after coextrusion with polystyrene, Hostyren N3000, as a function of the measured core melt temperature (see text for discussion).

By varying the temperature profile over the extruder that supplies the core melt and the coextrusion die, samples could be taken at different core melt temperatures (measured with a thermocouple, mounted perpendicular to the flow direction). The core material of these samples was tested for its crystalline melting point by means of DSC-analysis.
The results of the melting point measurements are presented in figure 6.8 as a function of the measured core melt temperature.
Again, as in the case of the POM/PS combination (see above) there appears to be a maximum in the ordering (assuming that both Young's modulus and melting point are reliable measures for molecular ordering). However, WAXS analysis of the sample with the highest melting point showed no sign of crystalline orientation whatsoever.
Hence it can be concluded that no ECC configuration was formed during the coextrusion process.

6.3 *Batch-wise extrusion of dispersions*

Again, for these experiments the capillary rheometer with a barrel diameter of 20 mm was used. Samples of polymer mixtures were prepared following the same procedure as described in section 4.5.1.

1) Continuous phase: LDPE, Stamylan 3400, MFI = 4.4 dg/min (2.16 kg at 190°C); particle size 3-4 mm.
   Dispersed phase: HDPE, Manolene 6003, MFI = 0.3 dg/min (2.16 kg at 190°C), with 0.02 weight % blue pigment (Horna PO 125, a phtalocyanine compound); particle size 0.5-1 mm.
   Mixture composition: 10 weight % HDPE in LDPE.
   Temperature: 130 ± 2 °C.
   Capillary: conical entrance (90°), D_c = 1.634 mm, L_c = 15.0 mm.
   Selective solvent for LDPE: decalin at 90°C.

At shear rates ranging from 2 to 40 s^{-1} the extrudate contained regular fibers with a reasonable parallel alignment; the fiber diameter ranged from 0.01 to 0.5 mm while the thinnest fibers were found in the centre of the extrudate. Analysis of these thin fibers

showed a high degree of orientation as shown in by Wide Angle X-ray Scattering (WAXS).
The thicker fibers showed no striking orientation, at least as could be detected by WAXS analysis. This result might be explained by the fact that during the experiment the highest stretching rates occur in the centre of the cone.
One might suggest that the small amount of pigment in the dispersed phase influenced the balance between deformation, relaxation and crystallization, probably by accelerating the crystallization; however, no proof for this assumption was found: the anomalous behaviour upon extrusion just above the melting point of the material, as decribed in section 3.1, was not found to be influenced by addition of the pigment. Moreover, the crystalline orientation of a cocontinuously extruded thread of the same material following the procedure as described in section 6.1 could not be improved by addition of the pigment.

2) Continuous phase: PS, Hostyren N5000, MFI = 3.5 dg/min (5 kg at 200°C), particle size $\leq$ 2 mm.
Dispersed phase: PP, Carlona P F6100, MFI = 0.5 dg/min (2.16 kg at 230°C), particle size 0.84-1.68 mm.
Mixture composition: 20 weight % PP in PS.
Temperature: 169°C (barrel), 160°C (capillary).
Capillary: conical entrance (90°), D_c = 1.634 mm, L_c = 30 mm.
Selective solvent for PS: chloroform.

At shear rates of 20 s^{-1} a thread containing regular PP-fibers was extruded. Upon DSC-analysis, apart from the "normal" melting peak at 160 ± 2 °C a substantial melting peak at 178 ± 2 °C was detected. This result could be reproduced within several test runs. In all cases the working pressure fluctuated roughly between 40 and 50 MPa. This is remarkably high compared to a pressure of 10 MPa needed for the extrusion of pure PS, Hostyren N5000, under exactly the same temperature and shear rate conditions.
Assuming the orientation-induced crystallization being favoured by a high pressure the capillary rheometer was fitted with the longest

capillary (d = 1.634 mm, l = 75.0 mm). Under the same conditions as described above at severely fluctuating pressures higher than 50 MPa, a thread containing PP-particles and no fibers was extruded. However, DSC-analysis yielded melting peaks of 169 ± 2 and 182 ± 2 °C, although no elongation whatsoever seemed to have taken place.

WAXS-analysis of the fibers from the first tests showed a substantial degree of orientation, as can be clearly seen from the diffraction pattern, shown in figure 6.9a. WAXS-analysis of the PP-particles, as formed in the experiment with the longest capillary, showed no remarkable orientation, although the corresponding melting point appeared to be higher (see figure 6.9b).

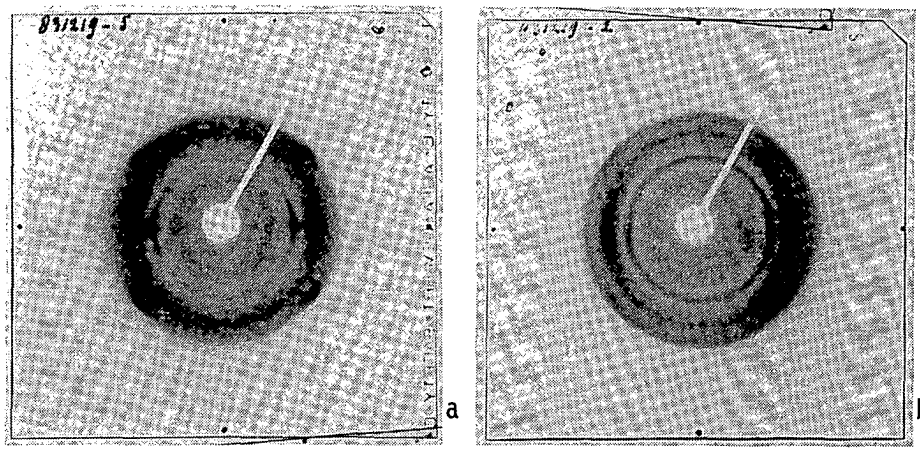


Fig.6.9 WAXS-pattern of PP, extruded as a dispersion in PS; a: fibers, b: particles (see text for discussion).

From these results it can be concluded that a high melting point does not automatically imply a high degree of crystalline orientation; a more probable assumption would be a high degree of molecular ordering at random crystalline orientation.

One possible explanation of this result might be that the initially highly oriented structure has been destroyed by melt fracture (see discussion in section 4.5.3); however, the appearance of the extrudate provided no evidence for this assumption. Another option is, that initially the PP-molecules were ordered and oriented to a high degree as a result of the combination of elongation and high pressure; if

this ordering and the corresponding deformation were of a predominantly elastic nature the orientation might have disappeared by elastic recovery upon exit from the capillary, while the ordering was retained on a smaller length scale and in different directions.

6.4 *Milling of dispersions*

Upon milling polymer mixtures, by varying the conditions (absolute and relative roll speed, temperature, gap width, and the properties of the materials themselves) different morphologies can be formed. For instance, if one of the two phases possesses a yield stress, processing under relatively mild conditions might give rise to the formation of a bicontinuous system or, to put it in other words, an interpenetrating network of both phases [73].
Another option is the formation of a fiber-reinforced blend (which can actually be regarded as being almost a bicontinuous system). Again, like in the examples described above, a number of scouting experiments were performed where the only aim was to investigate whether the formation of extended-chain crystalline fibers is possible in principle with the aid of this processing method.
For these experiments a small laboratory mill with a roll diameter of 100 mm and a roll breadth of 175 mm, variable roll speeds and gap widths, and with an adapted temperature control (to avoid overshoot) was used.

1) Continuous phase: SAN, Tyril LST 98 (?), properties not known.
   Dispersed phase: PVDF, Solef 1010, MFI = 1.0 dg/min (2.16 kg at 230°C.
   Mixture composition: 15 weight % PVDF in SAN.
   Temperature: 185°C (mixing), 160°C (crystallization).
   Roll speed: various, 1 : 1.
   Gap width: various.
   Selective solvent for SAN: chloroform.

After conditioning of the roll temperature at 185°C the mixture of SAN and PVDF granules was added to the rotating mill. The temperature

controls were immediately set to 160°C and the whole system was allowed to cool down (taking approximately 10 minutes). The relatively short time at high temperature was sufficient to allow complete melting of the PVDF.

On reaching the low temperature the rolls were kept rotating for another 10 minutes approximately. During this period, besides a very fine dispersion of PVDF in SAN, almost instantanuously a thin film of pure PVDF was formed on one of the rolls. After quenching the mixture on the rolls the SAN was selectively dissolved and the resulting PVDF-film was examined by DSC- and WAXS-analysis.

The first scan in the DSC-analysis showed two peaks; the first at 178 ± 2 °C, and the second at 183 ± 2 °C. A second scan of the same sample after solidification in the DSC-unit yielded the "normal" melting temperature for PVDF of 170 ± 2 °C.

WAXS-analysis showed a high degree of crystalline orientation, as is clearly depicted by figure 6.10a. Figure 6.10b shows the WAXS-pattern of a slightly oriented PVDF-sample formed at higher temperatures.

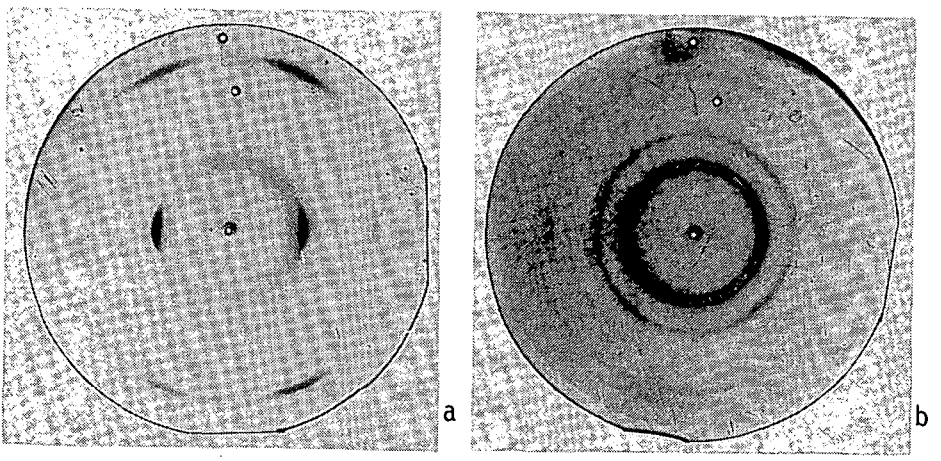


Fig.6.10 WAXS-pattern of PVDF-film formed by milling with SAN; a: highly oriented structure formed at 160°C, b: slightly oriented formed at higher temperatures (see text for discussion).

Variation of roll speed and gap width seemed to have hardly any influence on the results as detected by DSC- and WAXS-analysis. However, the best process stability could be achieved at roll speeds of 20 rpm and a gap width of 2 mm.

Addition of 3 - 25 weight % Cu-powder raised the temperature at which the highly oriented PVDF-film was formed, from 160°C to approximately 176°C. This result indicates that the presence of a heterogeneous nucleation site (as is also the roll surface!) plays an important role in this process.

Also in these experiments the initial goal, achieving self-reinforcement in a polymer blend by the formation of strong and stiff fibers, has not been realized.

7 Conclusions

From the numerous experiments as performed in the framework of this project, no proof is found for the possibility of realizing continuous production of strong and stiff polymer fibers or threads by orientation-induced crystallization in flowing two-phase polymer systems. Although the results of scouting experiments were sometimes encouraging, no reproducability was found in the cases where truly oriented crystal morphologies were formed. Moreover, in many cases upon approaching the conditions at which the desired effect was expected to happen, the experiment was partially or totally spoiled by flow instability problems.

On the other hand there is no proof either for the impossibility of the realization of such a process; one might say that it is just a case of bad luck that in this work the problem has mainly been approached from a rheological point of view (e.g. the balance between deformation and relaxation time scales). By now the idea that the crystallization kinetics play a key role in the process is becoming of more and more importance.

Evidence for the important role of the crystallization kinetics is found in this thesis as well as elsewhere. A number of arguments will be summed up here.

- During the milling experiments (section 6.5), the temperature at which crystallization in the highly oriented state takes place could be increased by adding 15 weight % of Cu-powder, indicating that heterogeneous nucleation sites can be of an enormous help (the oriented film was formed at the roll surface anyway). Increasing processing temperatures lead us further away from the flow instability regions.
- McHugh and coworkers [36,37] have shown that placing a number of needles in a tapered extrusion die allows for production of highly oriented fibers from a polymer "dispersion", although not (yet) continuously. Here again the stainless steel needles act as nucleation sites in the flowing polymer. Moreover, at the tip of the needles an extra elongational flow field is induced.

- In any experiment performed in the scope of this work, the anomalous behaviour as described in section 3.1 could not be realized with the same material when it was dispersed in or surrounded by another polymer melt that remains fluid under the specific conditions. One can easily understand that the lack of direct contact between the crystallizable melt and the die wall gives rise to a deviating behaviour, assuming the wall to play a role as a heterogeneous nucleation site. Instead of finding a way for continuous production of strong and stiff fibers by adding a second component, we spoil it all by shielding the crystallizable polymer melt from the position where crystallization would normally be initiated.

These considerations lead to a different interpretation of the results of Van der Vegt and Smit [31]. These authors suggested that the onset of crystallization occurs at the centre line in the conical entrance zone, where the rate of elongation is highest. The above arguments now lead us to the following interpretation:

- Upon extrusion of a crystallizable polymer melt with the aid of a capillary rheometer just above its melting point, as a result of the elongational flow in the entrance zone the polymer molecules are stretched and become highly oriented. In this oriented state they enter the capillary, where they undergo an extra shear field. As a result of both effects crystallization in an extended-chain conformation is induced at the capillary wall. Consequently, the effective capillary diameter decreases, as can be confirmed by an increasing pressure drop over the capillary (thus being not a result of an increasing viscosity caused by the onset of crystallization in the bulk); the shear stress increases, more molecules are incorporated in the ECC-lattice until ultimately the capillary is totally blocked and the flow ceases.

Solid proof for this explanation can only be found by performing a vast number of experiments with any kind of needles mounted in the die. The coextrusion set-up is extremely suitable for this purpose; given time, these experiments will surely be performed in the future.

If succesful this route might lead to the production of highly oriented and therefore strong and stiff polymer threads coated with another polymer.

To avoid the difficulties that arise in the case of a too high temperature, where relaxation of the induced orientation occurs before crystallization is allowed to take place, one can think of testing materials that consist of rigid-chain molecules and that consequently exhibit liquid crystal behaviour in the molten state under certain conditions for introduction in the process under consideration. Using essentially the same route, the initial ideal of realizing self-reinforcement of a polymer blend during processing might still be possible.

References

[1] Zachariades, A.E., W.T. Mead and R.S. Porter, in Cifferi, A. and I.M. Ward (eds.), "Ultra-High Modulus Polymers", Applied Science London (1979), 77.

[2] Porter, R.S., in Clason, C. and J. Kubat (eds.), Proc.Int.Congr. Rheol. 7th (1976), 120.

[3] Zachariades, A.E., W.T. Mead and R.S. Porter, Chem.Rev. 1980, **80**, 351.

[4] Kojima, S. and R.S. Porter, Thermosets High Perf. Thermoplast. (1977), 78 (Reg.Tech.Conf., Conn.Sect., Soc.Plast.Eng.).

[5] Southern, J.H. and R.S. Porter, J.Macromol.Sci. 1970, **B4**, 541

[6] Capiati, N.J., S. Kojima, W.G. Perkins and R.S. Porter, J.Mater. Sci. 1977, **13**, 334.

[7] Porter, R.S., N.E. Weeks, N.J. Capiati and R.J. Krzewki, J.Therm.Anal. 1975, **8**, 547.

[8] Capiati, N.J. and R.S. Porter, J.Polym.Sci.,Polym.Phys.Ed. 1977, **15**, 1427.

[9] Watts, M.P.C., A.E. Zacheriades and R.S. Porter, J.Mater.Sci. 1980, **15**, 426.

[10] Balta-Calleja, F.J., D.R. Rueda, R.S. Porter and W.T. Mead, J.Mater.Sci. 1980, **15**, 765.

[11] Capaccio, G., A.G. Gibson and I.M. Ward, in Cifferi, A. and I.M. Ward (eds.), "Ultra-High Modulus Polymers", Applied Science London (1979), 1.

[12] Ward, I.M., Philos.Trans.R.Soc.London, ser.A 1980, **294**, 473.

[13] Capaccio, G., T.A. Crompton and I.M. Ward, Polymer 1976, **17**, 664

[14] Capaccio, G. and I.M. Ward, Polym.Eng.Sci. 1975, **15**, 219

[15] Capaccio, G. and I.M. Ward, Polymer 1977, **18**, 967.

[16] Clark, E.S. and L.S. Scott, Polym.Eng.Sci. 1974, **14**, 682.

[17] Young, R.J. and C. Galiotis, Proc. IUPAC 1982 Amherst, 640.

[18] Young, R.J., R.T. Read, D.N. Batchelder and D. Bloor, Proc. of Conf. on Deformation, Yield and Fracture of Polymers, Cambridge 1982, 21.

[19] Iguchi, M., Brit.Polym.J. 1973, **5**, 195.

[20] Kunugi, T., A. Suzuki, I. Akiyama and M. Hashimoto, Polym.Prepr., Am.Chem.Soc.,Div.Polym.Chem. 1979, **20**, 778.

[21] Yamada, K., M. Kamezawa and M. Takayanagi, Polym.Prepr., Am.Chem. Soc.,Div.Polym.Chem. 1979, **20**, 780.

[22] Pennings, A.J. and K.E. Meihuizen, in Cifferi, A. and I.M. Ward (eds.), "Ultra-High Modulus Polymers", Applied Science London (1979), 117.

[23] Zwijnenburg, A., "Longitudinal Growth, Morphology and Physical Properties of Fibrillar Polyethylene Crystals", thesis Groningen State University, The Netherlands (1978).

[24] Zwijnenburg, A. and A.J. Pennings, Coll. and Polym.Sci. 1976, **254**, 868.

[25] Kalb, B. and A.J. Pennings, Polym.Bull. (Berlin) 1979, **1**, 871.

[26] Torfs, J.C.M. and A.J. Pennings, J.Appl.Polym.Sci. 1981, **26**, 303.

[27] Kalb, B. and A.J. Pennings, Polymer 1980, **21**, 3.

[28] Smook, J., J.C.M. Torfs, P.F. van Hutten and A.J. Pennings, Polym.Bull. (Berlin) 1980, **2**, 293.

[29] Keller, A., in Cifferi, A. and I.M. Ward (eds.), "Ultra-High Modulus Polymers", Applied Science London (1979), 321.

[30] Kalb, B. and A.J. Pennings, J.Mater.Sci. 1980, **15**, 2584.

[31] Van der Vegt, A.K. and P.P.A. Smit, S.C.I. 1967, monograph **26**, 313.

[32] Wunderlich, B., "Macromolecular Physics **3** (Crystal Melting), Academic Press New York (1980).

[33] Odell, J.A., D.T. Grubb and A. Keller, Polym.Eng.Sci. 1979, **19**, 433.

[34] Van der Vegt, A.K. and C.L.J.A. Verbraak, in Seferis, J.C. and P.S. Theocaris, "Interrelations between Processing, Structure and Properties of Polymeric Materials", Elseviers Science Publishers Amsterdam (1984), 57.

[35] Sakellarides, S.L. and A.J. McHugh, Polym.Eng.Sci. 1985, **25**, 1179.

[36] Sakellarides, S.L. and A.J. McHugh, Rheol.Acta 1987, **26**, 64.

[37] Tree, D.A. and A.J. McHugh, Intern.Polym.Processing II, 1988, **3**, 223.

[38] Bird, R.B., W.E. Stuart and E.N. Lightfoot, "Transport Phenomena", John Wiley & Sons New York (1960), 85.

[39] Han, C.D., "Multiphase Flow in Polymer Processing", Academic Press New York (1981).

[40] Maclean, L., Trans.Soc.Rheol. 1973, **17**, 385.

[41] Everage, A., Trans.Soc.Rheol. 1973, **17**, 629.

[42] Laven, J., "Non-Isothermal Capillary Flow of Plastics Related to their Thermal and Rheological Properties", thesis Delft University of Technology, The Netherlands (1985).

[43] Elmendorp, J.J., "A Study on Polymer Blending Microrheology", thesis Delft University of Technology, The Netherlands (1986).

[44] Taylor, G.I., Proc.Roy.Soc. (London) 1934, **A146**, 501.

[45] Cox, R.G., J.Fluid Mech. 1969, **37**, 601.

[46] Chaffey, C.E. and H. Brenner, J.Colloid Interface Sci. 1967, **24**, 258.

(47] Grace, H.P., Chem.Eng.Comm. 1982, **14**, 225.

[48] Bentley, B.J. and L.G. Leal, J.Fluid Mech. 1986, **167**, 241

[49] Van der Reijden-Stolk, C. and H. Boerstoel, to be published.

[50] Tsebrenko, M.V., A.V. Yudin, T.I. Ablazova and G.V. Vinogradov, Polymer 1976, **17**, 831.

[51] Tsebrenko, M.V., Intern.J.Polymeric Mater. 1983, **10**, 83.

[52] Narasaiah A. and J. Lyngaae-Jørgensen, Rheol.Acta 1980, **19**, 576.

[53] Vinogradov, G.V., N.P. Krasnikova, V.E. Dreval, E.V. Kotokova, E.P. Plotnikova and Z. Pelzbauer, Intern.J.Polymeric Mater. 1982, **9**, 187.

[54] Tsebrenko, M.V., N.M. Rezanova and G.V. Vinogradov, Polym.Eng. Sci. 1980, **20**, 1023.

[55] Vinogradov, G.V., B.V. Yarlykov, M.V. Tsebrenko, A.V. Yudin and T.I. Ablazova, Polymer 1975, **16**, 609.

[56] Ablazova, T.I., M.V. Tsebrenko, A.V. Yudin, G.V. Vinogradov and B.V. Yarlykov, J.Appl.Polym.Sci. 1975, **19**, 1781.

[57] Tsebrenko, M.V., Khimicheskie Volokna 1983, **3**, 28.

[58] Van Oene, H., J.Colloid Interface Sci. 1972, **40**, 448.

[59] Tsebrenko, M.V., N.M. Rezanova and A.V. Yudin, Khimicheskie Volokna 1979, **6**, 36.

[60] Lodge, A.S., Trans.Faraday Soc. 1956, **52**, 120.

[61] Leblans, P., "Constitutive Analysis of the Non-Linear Viscoelasticity of Polymer Fluids in Various Types of Flow", thesis Antwerp University, Belgium (1985).

[62] Wagner, M.H., Rheol.Acta 1976, **15**, 136.

[63] Wagner, M.H., J.Non-Newtonian Fluid Mech. 1978, **4**, 39.

[64] Wagner, M.H., Rheol.Acta 1979, **18**, 33.

[65] Wagner, M.H., T. Raible and J. Meissner, Rheol.Acta 1979, **18**, 427.

[66] Te Nijenhuis, K., "Dynamic Mechanical Studies on Thermo-Reversible Ageing Processes in Gels of Polyvinyl Chloride and of Gelatin", thesis Delft University of Technology, The Netherlands (1979).

[67] Scholtens, B.J.R. and H.C. Booij, in Mark, J.E. and J. Lal (eds.), "Elastomers and Rubber Elasticity", Am.Chem.Symp.Ser. 139, American Chemical Society, Washington D.C. (1982), 517.

[68] Williams, M.L. and J.D. Ferry, J.Polym.Sci. 1953, **11**, 169.

[69] Verbraak, C.L.J.A., K. te Nijenhuis and A.K. van der Vegt, Makromol.Chem., Macromolecular Symposia 1988, **16**, 361.

[70] Te Nijenhuis, K. and C.L.J.A. Verbraak, J.Non-Newtonian Fluid Mech., in press.

[71] Verbraak, C.L.J.A., J. van Dam and A.K. van der Vegt, Polym.Eng. Sci. 1985, **25**, 431.

[72] Marton, L. and C. Marton (eds.), Methods of Exp. Physics 1980, **16B**, 73.

[73] Verhoogt, H., personal comm..

Summary

In this thesis a number of items are treated that play an important role in the process of self-reinforcement of polymer blends by orientation-induced crystallization.
After summing up a number of methods that lead to the formation of highly oriented and therefore strong and stiff polymer structures, an analysis of the process of orientation-induced crystallization in a polymer melt is given in terms of a balance between deformation, relaxation and crystallization time scales. Deformation phenomena in two-phase polymer systems and the relaxation behaviour of a stretched polymer melt have been studied.
Cocontinuous, concentric two-phase polymer flow through a cylindrical channel is analysed with different models, and theoretical predictions are compared with experimental data. Results based on the power law model give the best description of the experimental observations.
General conditions for fiber formation from a dispersion as presented in literature are compared with experimental data. They appear not to be generally valid and can be influenced by process geometry.
The relaxation behaviour of a stretched polymer melt can be predicted to a fair extent with the aid of Wagner's constitutive equation, as can be concluded from an experimental study.
A large number of scouting experiments have been performed; in some cases the results were encouraging, but realization of a continuous process for the production of strong and stiff polymer fibers or threads from the melt has not been possible until now.
A minor process adaption is suggested, based on a slightly different interpretation of the anomalous behaviour that is found upon extrusion of a pure crystallizable melt just above its melting point.

Samenvatting

In dit proefschrift worden een aantal onderwerpen behandeld die een belangrijke rol spelen bij zelfversterking van polymeermengsels door oriëntatie-geïnduceerde kristallisatie.
Na een opsomming van een aantal methoden die leiden tot vorming van hoog-geörienteerde en daardoor sterke en stijve polymeerstrukturen wordt een analyse van oriëntatie-geïnduceerde kristallisatie gegeven aan de hand van een balans tussen deformatie-, relaxatie- en kristallisatie-tijdschalen. In dit werk zijn het deformatiegedrag van polymere tweefasensystemen en het relaxatiegedrag van verstrekte polymeersmelten bestudeerd.
Cocontinue concentrische tweefasen polymeerstroming door een cylindrisch kanaal wordt geanalyseerd aan de hand van verschillende modellen, en theoretische voorspellingen worden vergeleken met experimentele gegevens. De voorspellingen, gebaseerd op het Power-law model, vertonen de beste overeenstemming met de waarnemingen.
De in de literatuur gepresenteerde algemene condities voor vezelvorming uit polymeerdispersies worden vergeleken met experimentele gegevens. Zij blijken niet algemeen geldig te zijn en ze kunnen worden beïnvloed door de geometrie van de gebruikte opstelling.
Uit een serie experimenten blijkt dat het relaxatiegedrag van een verstrekte polymeersmelt redelijk voorspeld kan worden met behulp van de constitutievergelijking van Wagner.
Er zijn een groot aantal systematische verkennende experimenten uitgevoerd; in sommige gevallen waren de resultaten bemoedigend, maar de realisatie van een continu proces voor de produktie van sterke en stijve polymeervezels of -draden uit de smeltfase is tot op heden niet mogelijk gebleken.
Gebaseerd op een enigszins andere interpretatie van het afwijkende gedrag dat wordt gevonden bij extrusie van een kristalliseerbare smelt net boven het smeltpunt wordt een kleine aanpassing van het proces voorgesteld.

List of symbols

Latin characters:

a	radius of core melt
c_{ij}^{-1}	i,j-component of relative finger strain tensor
D_c	capillary diameter
E	flexural modulus
f	vibrational frequency
g	gravitational acceleration
G'	storage modulus
G''	loss modulus
$G_0(t)$	shear modulus
h	damping function
$H(\tau)$	relaxation time spectrum
I_1	first invariant of finger tensor
I_2	second invariant of finger tensor
K	power law constant
K_1	power law constant of matrix material
K_2	power law constant of core material
l	length
l_0	initial length
L_c	capillary length
$\bar{M}_w$	weight-average molecular weight
n	power law index
n_1	power law index of matrix material
n_2	power law index of core material
p_0	isotropic stress
p_{ij}	i,j-component of stress tensor
P	isotropic pressure
q_e	rate of elongation
r	radial distance
R	radius of droplet
R_1	radius of cylindrical channel
t	time
t'	time of deformation

t_0 beginning of flow
t_1 cessation of flow
T temperature
v velocity
v_1 velocity of matrix component
v_2 velocity of core component
$\underline{v}$ velocity vector
We Weber number $\eta_1 \dot{\gamma} R/\sigma$

Greek characters:

$\bar{\alpha}_0$ temperature coefficient of the viscosity
α_1 reciprocal power law index of matrix material $1/n_1$
α_2 reciprocal power law index of core material $1/n_2$
$\bar{\beta}_0$ pressure coefficient of the viscosity
$\dot{\gamma}$ shear rate
$\underline{\dot{\gamma}}$ shear rate tensor
δ loss angle
δ_{ij} Kronecker delta
ϵ Hencky strain $\ln l/l_0$
ϵ_{max} maximum Hencky strain
η (shear) viscosity
η_1 (shear) viscosity of matrix material
η_2 (shear) viscosity of core or dispersed material
λ diameter ratio or radius ratio a/R_1
μ memory function
ρ density
σ interfacial tension
τ relaxation time
τ_c crystallization time
τ_{cr} critical shear stress
τ_e time scale of experiment
τ_{lim} limiting shear stress
τ_{max} upper limit relaxation time spectrum
τ_{min} lower limit relaxation time spectrum

τ_r	relaxation time scale
τ_s	shear stress
$\underline{\underline{\tau}}$	stress tensor
ϕ	volume flux
ϕ_1	volume flux of matrix component
ϕ_2	volume flux of core component
Ψ_1	first normal stress difference coefficient
Ψ_2	second normal stress difference coefficient
ω_{max}	upper limit reduced frequency interval
ω_{min}	lower limit reduced frequency interval
$\underline{\underline{\omega}}$	vorticity tensor